



NYSLAB: SOFTWARE FOR ANALYSIS OF JOINTED PAVEMENTS

Conducted for:

**Engineering & Software Consultants, Inc.
14123 Robert Paris Ct.
Chantilly, VA 20151**

Research Report FHWA-RD-07-1008-01

December 2009

**Center for Transportation Infrastructure Systems
The University of Texas at El Paso
El Paso, TX 79968
(915)747-6925
<http://ctis.utep.edu>**

TECHNICAL REPORT STANDARD TITLE PAGE

1. Report No. FHWA-RD-07-1008-01	2. Government Accession No.	3. Recipient's Catalog No.	
4. Title and Subtitle NYSLAB: A SOFTWARE FOR ANALYSIS OF JOINTED PAVEMENTS		5. Report Date December 2009	
		6. Performing Organization Code	
7. Authors C. Carrasco, M. Limouee, M. Celaya, I. Abdallah and S. Nazarian		8. Performing Organization Report No. Research Report FHWA-RD-07-1008-01	
9. Performing Organization Name and Address Center for Transportation Infrastructure Systems The University of Texas at El Paso El Paso, Texas 79968-0516		10. Work Unit No.	
		11. Contract or Grant No. DTFH61-05-D0-00017	
12. Sponsoring Agency Name and Address Engineering & Software Consultants, Inc. 14123 Robert Paris Ct. Chantilly, VA 20151		13. Type of Report and Period Covered Final Report June 2006-December 2009	
		14. Sponsoring Agency Code	
15. Supplementary Notes Research Performed in Cooperation with FHWA. Contacting Agency: Engineering and Software Consultants, Inc. (FHWA)			
16. Abstract Researchers at the University of Texas at El Paso (UTEP) have been charged to implement several modifications in the latest version of JSLAB called JSLAB2004. A thorough review of JSLAB2004 source code that was developed in the 1970's revealed that it would be beneficial to recode the software completely to take advantage of the modern programming and finite element modeling (FEM) tools available today called NYSlab. The most significant improvements implemented in NYSlab over other software are: a) Finite Element model based on an isoparametric element that allows for the modeling of irregular geometries, b) no limitation in the number of PCC and foundation layers, c) more accurate modeling of the contact between unbonded PCC layers, PCC and foundation layers using Gap elements, d) foundation model extended beyond the edge of the slabs to more accurately model the edge deflections and stresses, and e) implementation of non-linear thermal gradient models applied to any number of PCC layers. The new code results compare well with the other codes and have good convergence characteristics. The parametric studies also demonstrate a well behaving code for various pavement-section configurations.			
17. Key Words Pavement Response, Jointed Pavement, PCC slabs, Finite Element Analysis, Superheavy Vehicles, isoparametric element, non-linear thermal gradient models		18. Distribution Statement No restrictions. This document is available to the public through the National Technical Information Service, 5285 Port Royal Road, Springfield, Virginia 22161, www.ntis.gov	
19. Security Classified (of this report) Unclassified	20. Security Classified (of this page) Unclassified	21. No. of Pages xvi, 63	22. Price

NYSLAB: A SOFTWARE FOR ANALYSIS OF JOINTED PAVEMENTS

by

**Cesar Carrasco, Ph.D.
Maryam Limouee, MSCE
Manuel Celaya, MSCE
Imad Abdallah, MSCE
and
Soheil Nazarian, Ph.D., P.E.**

Research Report FHWA-RD-07-1008-01

**Conducted for
Federal Highway Administration**

December 2009

The Center for Transportation Infrastructure Systems
The University of Texas at El Paso
El Paso, TX 79968-0516

The content of this report reflect the view of the authors, who are responsible for the facts and the accuracy of the data presented herein. The contents do no necessarily reflect the official views or policies of the Federal Highway Administration or participating States. This report does not constitute a standard, specification, or regulation.

NOT INTENDED FOR CONSTRUCTION, BIDDING, OR PERMIT PURPOSES

ACKNOWLEDGEMENT

The successful progress of this project could not have happened without the help and input of many New York State DOT, FHWA, Texas DOT, and Ohio DOT personnel. The authors acknowledge Dr. Julian Bendaña of NYSDOT for his guidance and valuable input. The interaction with Ms. Katherine Petros, Mr. Eric Weaver both from FHWA has been very beneficial to us. We also acknowledge very valuable input by Dr. Magdy Michael of TxDOT and Mr. Roger Green of ODOT.

We would like to acknowledge close collaboration that we enjoyed with Dr. Shad Sargand of Ohio University on this project.

EXECUTIVE SUMMARY

A significant amount of research and development has been conducted for decades to provide a tool for the design and analysis of jointed slabs on different types of foundations. JSLAB, which has been maintained by the Federal Highway Administration (FHWA) and is distributed free of charge, is one example of such programs. JSLAB has gone through several iterations of improvements in the last thirty years. There has been interest in further improving the capabilities of that software package in recent years..

Researchers at the University of Texas at El Paso (UTEP) have been charged to implement several modifications in the latest version of JSLAB called JSLAB2004. A thorough review of JSLAB2004 source code that was developed in the 1970's revealed that it would be beneficial to recode the software completely to take advantage of the modern programming and finite element modeling (FEM) tools available today. As such, a new code was developed in MATLAB that significantly enhances the efficiency and capabilities of JSLAB2004. The new software will be referred to as NYSlab hereafter.

The most significant improvements implemented in NYSlab over other software are: a) Finite Element model based on an isoparametric element that allows for the modeling of irregular geometries, b) no limitation in the number of PCC and foundation layers, c) more accurate modeling of the contact between unbonded PCC layers, PCC and foundation layers using Gap elements, d) foundation model extended beyond the edge of the slabs to more accurately model the edge deflections and stresses, and e) implementation of non-linear thermal gradient models applied to any number of PCC layers.

In addition to discussing the improvements to JSLAB2004 in this report, a comparison between the improved code and the other common codes is also presented. Several studies were conducted to determine the convergence characteristics of the new FEM formulation. Finally, several parametric studies were conducted to verify the appropriate behavior of the code for different geometric configurations, foundation models and parameters, and temperature gradient profiles.

These studies indicate that the new code results compare well with the other codes and have good convergence characteristics. The parametric studies also demonstrate a well behaving code for various pavement-section configurations.

TABLE OF CONTENTS

ACKNOWLEDGEMENT	VII
EXECUTIVE SUMMARY	IX
TABLE OF CONTENTS	XI
LIST OF TABLES	XIV
LIST OF FIGURES	XV
CHAPTER 1 – INTRODUCTION	1
1.1 Rigid Pavements Modeling.....	1
1.2 History of the Development of JSLAB.....	2
1.2.1 Development of ILLI-SLAB.....	2
1.2.2 Development of J-SLAB (1986).....	3
1.2.3 Development of J-SLAB92 (1992).....	3
1.2.4 Development of JSLAB2004 (2001-2004).....	4
1.2.5 Development of ISLAB2000	4
TABLE 1.1: HISTORY OF THE DEVELOPMENT OF J-SLAB [15]	5
CHAPTER 2: CHARACTERISTICS OF JOINTED PAVEMENTS	7
2.1 Foundation Types.....	7
2.1.1 Winkler Model	7
2.1.2 Boussinesq Model.....	8
2.1.3 Vlasov Model.....	9

2.1.4 Kerr Model.....	10
2.1.5 Zhemochkin, Sinitsyn and Shtaerman (ZSS).....	11
2.2 Load Transfer Devices.....	11
2.2.1 Aggregate and Key Interlock.....	12
2.2.2 Dowels and Ties.....	12
CHAPTER 3: THE FINITE ELEMENT CORE PROCESSOR	13
3.1 Pavement Section Modeling.....	13
3.1.1 Mindlin Plate Theory.....	13
3.1.2 Mindlin Plate Element.....	15
3.1.3 Foundation Elements.....	18
3.1.4 Load Transfer Elements.....	20
3.1.5 Gap Element.....	21
3.2 Load Vectors.....	21
3.2.1 Truck Loads.....	21
3.2.2 Thermal Loads.....	22
CHAPTER 4: CONVERGENCE STUDY	25
4.1 Number of elements.....	25
4.1.1 Single Slab Study.....	26
4.1.2 Control Case Study.....	27
4.2 Element Aspect Ratio.....	31
CHAPTER 5: COMPARISON STUDY	33
5.1 Description Of Case Study.....	33
5.2 Comparison.....	36
CHAPTER 6: PARAMETRIC STUDY	39
6.1 Foundation Parameters.....	39
6.1.1 Winkler Foundation.....	39
6.1.2 Vlasov Foundation.....	41
6.1.3 Solid Elastic Foundation.....	43

6.2	Foundation Model	45
6.3	Slab Dimensions	45
6.3.1	Slab Length and Width	45
6.3.2	Slab Thickness	49
6.3.3	Unbonded PCC Layers	49
6.4	Thermal Gradient	53
CHAPTER 7: SUMMARY AND CONCLUSIONS		57

LIST OF TABLES

Table 1.1: History of the development of J-SLAB [15]	5
--	---

LIST OF FIGURES

Figure 2.1 Slab on Winkler foundation [6].....	8
Figure 2.2 Deflection of the slab on Elastic Solid (ES) foundation [11].....	9
Figure 2.3 Slab on Pasternak foundation [6]	10
Figure 2.4 Slab on Kerr foundation [6].....	11
Figure 2.5 Aggregate interlocks [41].....	12
Figure 2.6 Application of dowels and tie bars [41]	12
Figure 3.1 Jointed slab pavement section in NYSlab	14
Figure 3.2 Quadrilateral elements with MITC tying points.....	18
Figure 3.3 Dowel bar Degree of Freedom	21
Figure 3.4 Shape Function N_1	22
Figure 4.1 Uniform (a) and non-uniform (b) meshes	25
Figure 4.2 Deflections convergences for single slab	26
Figure 4.3 Stress convergences for single slab	27
Figure 4.4 Scheme of the truck.....	29
Figure 4.5 Tire layout	29
Figure 4.6 Deflections convergences for control case.....	29
Figure 4.8 Stress convergences in the Y direction for control case.....	30
Figure 4.9 Deflections convergence as a function of element aspect-ratio	31
Figure 4.10 Stresses convergence as a function of element aspect-ratio.....	32
Figure 5.1 Truck dimensions	34
Figure 5.3 ISLAB2000 output (X-stress).....	35
Figure 5.4 NYSLAB MATLAB code output for top soil layer deflection.....	36
Figure 5.5 Deflections comparison.....	37
Figure 5.7 Comparisons of stresses in the Y direction	38
Figure 6.1 Maximum deflection as a function of modulus of sub-grade reaction.....	40
Figure 6.2 Maximum bending stresses as a function of sub-grade reaction.....	40
Figure 6.3 Deflection as a function of Vlasov parameters (k,G).....	41
Figure 6.4 Longitudinal stress in the X direction as a function of Vlasov parameters (k,G)	42
Figure 6.5 Longitudinal stress in the Y direction as a function of Vlasov parameters (k,G)	42
Figure 6.6 Deflection as a function of Solid Elastic parameters (E,v)	43
Figure 6.7 Longitudinal stress in the X direction as a function of Solid Elastic parameters (E,v).....	44
Figure 6.8 Longitudinal stress in the X direction as a function of Solid Elastic parameters (E,v).....	44

Figure 6.9 Effect of extending the foundation beyond the edge of the slab in the Vlasov model	46
Figure 6.10 Comparison of deflections under the Winkler, Vlasov and Solid Elastic foundations	47
Figure 6.11 Comparison of bending stresses (in X direction) under the Winkler, Vlasov and Solid Elastic	47
Figure 6.12 Deflection as a function of slab dimensions	48
Figure 6.13 Longitudinal bending stress in the X direction as a function of slab dimensions	50
Figure 6.14 Deflection as a function of PCC layer thickness	51
Figure 6.15 Longitudinal stresses as a function of of PCC layer thickness	51
Figure 6.16 Deflection as a function of top PCC layer thickness	52
Figure 6.17 Longitudinal stress in the X direction as a function of top PCC layer thicknesses	52
Figure 6.18 Longitudinal stress in the X direction as a function of top PCC layer thicknesses	53
Figure 6.19 Maximum deflection as a function of Linear Thermal Coefficient (a_1)	54
Figure 6.20 Maximum longitudinal stresses as a function of Linear Thermal Coefficient	54
Figure 6.21 Maximum deflection as a function of Quadratic Thermal Coefficient (a_2)	55
Figure 6.22 Maximum longitudinal stresses as a function of Quadratic Thermal Coefficient	55

CHAPTER 1 – INTRODUCTION

A number of analytical software tools for modeling jointed slabs on different types of foundations and their application in pavement design have been developed in the past decades. The finite element program ILLI-SLAB, which was developed for the structural analysis of one or two layered portland cement concrete pavements (PCCP) with or without mechanical load transfer system at joints and cracks, has been under continuous revision and verification to improve its accuracy and ease of use [5, 6, 9].

The finite element program JSLAB, which determines the stresses developed in rigid pavement under various loading conditions, was developed shortly after. JSLAB has been updated several times to incorporate thermal stresses, calculate the principal stresses, and search for the location and the value of the maximum stress. That version of the software was perceived as more user-friendly in comparisons with other software packages [9, 16].

The next generation of this software, JSLAB2004, incorporated an axel configuration library and an “Express Mode” interface. JSLAB2004 can be used to analyze jointed pavement responses under several loads for a two-layer system of up to nine slabs. Different kinds of joints can be uniformly or non-uniformly spaced. JSLAB2004 also provides the capability to calculate pavement response under a moving load.

In the following sections, the application of the finite element in analyzing the rigid pavements is discussed, and the available software for this purpose is introduced. A brief history of JSLAB development is also presented. ISLAB2000, which was developed to reduce or eliminate some of the limitations of the ILLI-SLAB, will be described also. These codes are discussed because they are the most widely used jointed-pavement analysis tools.

1.1 RIGID PAVEMENTS MODELING

Elastic layered programs (ELPs) are the most common programs used for design of pavements. The horizontal infinity assumption for the slabs makes these programs a reliable theoretical method for pavements without discontinuities, which are mostly classified as flexible pavements. In contrast, a portland cement concrete (PCC) pavement with joint connections naturally cannot

be considered as an infinite slab. The concept of semi-elastic half space used in ELPs is not applicable for rigid pavements. In rigid pavements, the tire proximity to the edges and the rigidity of the joints have a significant role in the mechanical performance of the system. Therefore, a more complex method is required to estimate the maximum bending stresses and deflections experienced by rigid pavements [2]. In addition, the contact between the slab and subgrade has a major effect on the rigid pavement performance. Pumping, temperature curling, and moisture warping cause a discontinuity between the slab and the subgrade that makes the analysis of the pavement a non-linear problem. This complex behavior can only be modeled using numerical algorithms like the finite element method (FEM) [2, 5, 10].

1.2 HISTORY OF THE DEVELOPMENT OF JSLAB

In 1965, Cheung and Zienkiewicz added the stiffness coefficients of the foundation to analyze the stiffness of the slabs on liquid and solid elastic foundation by using FEM [11]. Huang and Wang used the FEM in early 1970's, for the analysis of jointed slabs on liquid foundations. Huang further applied the method to jointed slabs on solid foundation in 1974 [5]. In the same year, Huang and Wang used FEM for concrete slabs having partial contact with the foundations [12]. This research resulted in the development of the WESLIQUID program by Huang and Chou [5, 13]. WESLIQUID was able to calculate the stresses and deflections in concrete pavements and the subgrade with or without joints and cracks. In 1981, the Waterways Experiment Station developed the WESLAYER program for analyzing layered elastic solids that model various foundation layers [13].

Tabatabaie and Barenberg developed ILLI-SLAB at the University of Illinois in the late 1970s [14]. This FEM software became the basis of JSLAB, which was developed in 1986 for the Portland Cement Association by Tayabji and Colley [5].

1.2.1 Development of ILLI-SLAB

The first development of the FEM for analyzing rigid pavement slabs was done at the University of Illinois. The result was ILLI-SLAB, a finite element program that was written in FORTRAN [14]. ILLI-SLAB used a rectangular 4-noded element with 12-degrees-of-freedom first developed by Melosh [25]. Each node has three degrees of freedom: w , the vertical deflection in z -direction, a rotation θ_x about x -axis and rotation θ_y about y -axis [6, 9, 15, 25].

Since the first version of ILLI-SLAB by Tabatabaie and Barenberg researchers at the University of Illinois have implemented many improvements to make it more user-friendly and enhance its capabilities [2, 5, 6, 9, 10]. The first foundation model used in ILLI-SLAB was a Winkler foundation, modeled as vertical spring elements. One of the improvements to this software was the inclusion of new foundation models, such as the elastic solid foundation. ILLI-SLAB was the first program that had both types of ideal subgrades (liquid and solid elastic) in one package [2, 10].

Cauwelaert *et al.* worked on solutions for analyzing the infinite and semi-infinite slabs on the so-called Pasternak foundations [6]. To determine the parameters for a Pasternak Foundation, a back-calculation procedure developed by Stet and his colleagues was used [37]. Cauwelaert's closed forms solution assumes full contact between the slab and the foundation and can only analyze the effects of wheel loading [6].

The assumptions used for the analysis of PCC layers in ILLI-SLAB were based on the classical medium-thick elastic plate theory. The medium-thick plate theory is able to model out-of-plane transverse forces through flexure, but is not thick enough for the shear deformation to be important [2]. Such a plate adheres to Kirchhoff's Theory (small deformation theory), in which the normal plane that is perpendicular to the middle surface of an undeformed plate will also be plane and perpendicular to the middle surface of the deformed plate. In that theory the layers parallel to the middle surface follow the plane stress theory and the load will not cause any axial or in-plane shear stresses [2, 10, 25].

ILLI-SLAB can analyze any configuration of loads. To convert external loads to nodal loads, ILLI-SLAB uses a work-equivalent load vector. This program can also calculate stresses due to a temperature difference between the top and the bottom of the slab. Different types of pavement configurations are available in ILLI-SLAB, such as bonded or un-bonded layers (PCC to PCC, PCC to subgrade or PCC to overlay). In the case of bonded conditions, the interface is designed as fully strain compatible, and for unbonded cases, shear stresses at the interface are neglected. ILLI-SLAB is able to process the analysis of several slabs with or without mechanical load transfer systems at the joints. The mechanical load transfer system can consist of aggregate interlock, dowels, or a combination of these two. Aggregate interlock transfers the loads through shear, while dowel bars carry some moment as well as shear. The dowels are located at the neutral plane of the slab and are designed as linear elastic tools [2, 6, 9, 10].

1.2.2 Development of J-SLAB (1986)

Tayabji and Colley developed JSLAB to compute the critical stresses and deflections in rigid pavements under different loading conditions [5]. This software was based on an early version of ILLI-SLAB and used the Portland Cement Association's (PCA), thickness-design procedure that was revised in 1984 for jointed plane concrete pavements (JPCP), jointed reinforced concrete pavements (JRCP), and continuously-reinforced concrete pavements (CRCP). To determine the thermal stresses in this first version of JSLAB, the program had to be executed twice. In that version the curling analysis could only be done for a single slab. In addition, the first version of JSLAB was also not able to calculate subgrade stresses. However, the JSLAB program was able to analyze square and round dowels, in contrast with ILLI-SLAB, which was capable analyzing round dowel bars only [5], [9].

1.2.3 Development of J-SLAB92 (1992)

An error in the curling formula was corrected and verified by theoretical and numerical comparisons in JSALB92. This version of JSLAB was able to calculate the principal stresses,

and it was also capable of searching for the location and value of the maximum stress. In J-SLAB 92, the stiffness matrix of the dowel bar was corrected to accurately satisfy the equilibrium conditions. Also, an additional step for the calculation of self-weight deflections was added to the curling analysis [4].

1.2.4 Development of JSLAB2004 (2001-2004)

Several improvements were made to JSLAB92 that resulted in JSLAB2002 followed by JSLAB2004. JSLAB2002 could analyze six different subgrade types:

1. Spring foundation (SP)
2. Winkler foundation (Dense Liquid [DL] model)
3. Boussinesq foundation (Elastic Solid [ES] model)
4. Vlasov Two-Parameter (TP) foundation
5. Kerr Three-Parameter (K3) foundation
6. Zhemochkin-Sinisyn-Shtaerman (ZSS) foundation [4]

The user manual and graphic interface of JSLAB2002 with pre- and post-processors made it more user-friendly than the earlier versions. This version was tested by comparing it with BISAR, the FAA's H51, J-SLAB 92, and with pavement test data that was obtained at the Ohio Test Road [4].

The "Express Mode" option was added to JSLAB2004 to accommodate more user needs. This version of JSLAB had an axle library including single, dual, and super single tires and tandem, triple and quad axle configurations. The "Express" interface generated input data in a more user-friendly way and allowed users to easily change the loading areas, axle spacing, and move the axle groups to any position on the slab.

JSLAB2004 is capable of analyzing the jointed pavement under self-weight, traffic load, and a combination of these two. Temperature gradient or any combination of temperature gradient and traffic load can also be calculated for a single slab. JSLAB2004 can analyze up to a two-layer pavement system and can consider fully bonded or fully unbonded systems with a limitation of the three slabs in each direction (nine slabs in total). The software also allows for the modification, on a per-element basis, of material properties, slab thicknesses, and support conditions. Uniformly or non-uniformly spaced, circular, or non-circular dowels, tie bars, and aggregate interlocks are the options for modeling of joints in JSLAB2004. The "Time History" analysis under a moving load at specified locations was another feature added to JSLAB2004. That version can also analyze multiple-slab curling [4]. A brief summary of the J-SLAB development history is presented in Table 1.1.

1.2.5 Development of ISLAB2000

ILSL2 and ISLAB2000 are two different FEM codes which were developed to reduce or eliminate some of ILLI-SLAB limitations. By introducing semi-infinite elements in one or two horizontal dimensions in ILSL2, Khazanovich and Ioannides [6] were able to overcome a major

Table 1.1: History of the development of J-SLAB [15]

Version	Year	Creditors	Modification and Improvement
ILLI-SLAB	1977	Tabatabaie & Barenberg	Original version
	1980	Wang	Revision
	1983	Ioannides	Several subgrade models included
	1984	Conroyd	Adapted to ANSI-77 FORTRAN
	1989	Korovesis	A new procedure for curling analysis incorporated.
	1994	Khazanovich	ILSL2, New generation of the program
J-SLAB	1986	Tayabji	<ul style="list-style-type: none"> • A program for analysis of jointed concrete pavements. • Version in FORTRAN.
J-SLAB 92	1992	Dong	<ul style="list-style-type: none"> • Added thermal stress in the stress expression. • Corrected dowel bar stiffness matrix to satisfy the equilibrium condition. • Added calculation of principal stresses, searching for location and value of maximum stress • One-step procedure replaced two-step procedure to treat the self-weight in curling analysis.
JSLAB2004	2001-2004	Galaxy Scientific Corp.	<ul style="list-style-type: none"> • Upgraded the types of base/subgrade foundations including Winkler, spring, Boussinesq, two-parameter, three-parameter and ZSS foundations. • Developed user Friendly graphical user interfaces. • Installed a library of axle configurations and vehicles. • Added capability to calculate the response time history under the moving axle loads or a vehicle. • Version in Visual Basic 6

limitation of ILLI_SLAB. This finite element program used Toksky [7] model to analyze interior loading cases more accurately by considering the effects of subgrade deformation under slab edges. ILSL2 offered a variety of subgrade options such as the Kerr model and the Zhemochkin, Sinitsyn and Shtaerman model. The Pasternak or Kerr model for subgrade characterization could be used to analyze one single slab. Curling stresses, which have a significant effect on PCC pavements performance, cannot be evaluated by analyzing a single slab, as it will omit load transferring behavior at the joints. Khazanovich and his colleagues developed ISLAB2000 which had all the positive features of ILSL2 but was free of some unnecessary limitations (such as limitations on the number of nodes in a finite element model). The program was developed by the ERES Division of Applied Research Associates (ARA), with support from the Michigan Department of Transportation and the Minnesota Department of Transportation [6, 7, 8, 15].

One of the improvements made during ISLAB2000 development was enabling curling analysis of slabs on the Pasternak and Kerr foundations. To do this, it was assumed that the slab and the subgrade are separated if there is a tensile stress between them. Erland *et al.* [3] found that in comparison with J-SLAB 92, in which mechanistic response predicts higher strains for rigid pavement than measured in the field, ISLAB2000 results are more similar to field-measured data [6].

Rewriting of the code improved the software's ability in analyzing mismatched joints and cracks, voids, mesh generating, load placement, and batch processing. Moreover, ISLAB2000 can solve pavement responses due to temperature, traffic, and construction loading. Also, its graphical user interface (GUI) for input and output make it more user-friendly [1, 5].

CHAPTER 2: CHARACTERISTICS OF JOINTED PAVEMENTS

A significant amount of research work has been conducted with the intent of finding models that describe the elastic and plastic behavior of beams and slabs on linear and non-linear foundations. A brief description of the most common foundation models used in the modeling of PCC slabs as well as a description of the load transfer devices used in jointed pavements will be presented in this section.

2.1 FOUNDATION TYPES

The following is a detailed description of the elastic foundation models currently used in JSLAB and also implemented in NYSlab.

2.1.1 Winkler Model

Westergaard published his first paper on the analysis of concrete pavements in 1923 and twenty-five years later he published his last research results on “slab-on grades” in 1948 [5]. In both papers, assuming some restrictions, he modeled the rigid pavement as a plate on a bed of springs. Westergaard developed temperature-curling equations, and through his theoretical studies on the stress and deflections in concrete pavements, determined pavement performance equations for loading near corner, an edge, and at the interior of a large slab. In his analyses, he assumed that the foundation spring at one point was independent of the others and slab subgrade reactive pressure was proportional to the deflection of the spring at that location. As a result, in 1961, Winkler created a foundation model which was a combination of a series of independent springs [5, 6, 10, 15, 31]. Figure 2.1 shows a slab on Winkler foundation. These springs have an axial stiffness defined as:

$$K=A*k \tag{2.1}$$

where K is stiffness of the equivalent spring, k is the parameter of the Winkler model, and A is the area of the subgrade.



Figure 2.1 Slab on Winkler foundation [6]

The Winkler foundation is also referred to as a dense liquid (DL) foundation, where the displacement is proportional to the total load applied. In other words, the term "liquid" does not refer to an absence of shear strength, but it means the slab is placed on an infinite number of springs, and the total volume of displacement is proportional to the total load applied. This assumption makes the Winkler model, the simplest foundation model with one parameter, k , which is the modulus of subgrade reaction. This modulus is usually obtained from the plate load test, and it is sensitive to the radius of the plate used in its determination. The modulus k is assumed to be independent of stress and deflection level, but most subbase/subgrade support systems have a stress-dependent load-deformation response [5, 6, 7, 10].

Westergaard assumed that a medium thick plate (where shear deformations ignored) for the PCC slab was sufficient; he also assumed that the slab and subgrade were in full contact. This foundation is able to model the scenario of the critical load transferred at PCC slab joints, and develop distresses, such as faulting, pumping and corner breaking [7].

2.1.2 Boussinesq Model

The Winkler model was mentioned as being the simplest representation of a continuous elastic foundation; this foundation used approximations to avoid mathematical difficulties for cases with continuous foundations. Cheung and Zienkiewicz [11] showed that the actual subgrades behave more like an elastic solid rather than a liquid [5, 10, 23]. Pickett *et al.* [24] developed theoretical solutions for concrete slabs on an elastic half-space. Their research resulted in design charts for concrete pavements [23].

The following equation was developed by Giroud, which was used in ILLI-SLAB to calculate the deflection over an elastic solid foundation:

$$w_{ij} = \frac{F_j (1 - \nu_f^2)}{\pi E_f r_{i,j}} \quad (2.2)$$

where w_{ij} is deflection at position i due to force at position j , F_j is the force at position j , $r_{i,j}$ is the distance between positions i and j , and E_f , and ν_f are modulus of elasticity and the Poisson's ratio of the foundation, respectively. The deflection at the center of a rectangular loaded area can be calculated as follows:

$$w_{ii} = 2 \int_{\xi=0}^{\xi=a/2} 2 \int_{\eta=0}^{\eta=b/2} \frac{P_i (i - \nu_o^2)}{ab\pi E_o} \frac{d\xi d\eta}{\sqrt{(\xi^2 + \eta^2)}} \quad (2.3)$$

where P_i is the distributed load over the rectangular element with dimensions \mathbf{a} by \mathbf{b} (see Figure 2.2). For a point outside the rectangular loaded area, the deflection can be calculated using Equation 2.2 replacing the rectangular load with the resultant force F . Cheung and Zienkiewicz [11] showed that this approximation is adequate with a less than 5% error. As shown in Figure 2.2, the deflection at a given point relates to the forces at all other points on the foundation. Therefore, calculating the stiffness matrix for this continuous foundation is possible through inversion of the flexible matrix, which is obtained using Boussinesq's Theory described in Equations 2.2 and 2.3 [5, 10].

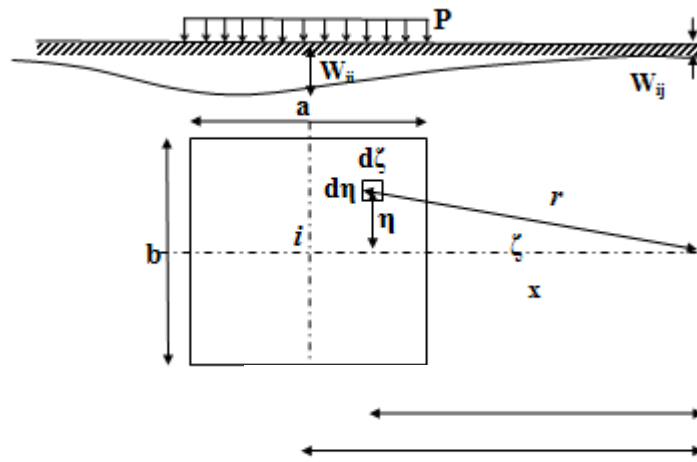


Figure 2.2 Deflection of the slab on Elastic Solid (ES) foundation [11]

Cheung and Zienkiewicz proposed a method for incorporating the elastic solid subgrade in a two-dimensional plate bending finite element model for the first time [11]. Their solution for this problem was as complete as the Westergaard solution. To introduce soil nonlinearity, Thompson and Robnett proposed a resilient modulus characterization for the elastic solid foundation [10].

The shear interaction described by the Boussinesq model is stronger than usually observed in the field. Since Boussinesq is a continuum model, it is not well suited for implementation on previous FEM packages that directly add the foundation stiffness to the slab stiffness [6, 7].

2.1.3 Vlasov Model

Because the Winkler foundation model assumes that the deflection at one point is independent of the deflection everywhere else (springs are not coupled), the model is incapable of capturing the foundation deformation beyond the edge of the slab. This deformation decays at some distance but still can have a significant effect on edge stresses and deformations. By connecting the top of the Winkler springs to an incompressible layer of vertical elements, Pasternak proposed a model

that deforms by lateral shear only. Vlasov developed a model that includes shear interaction between soil elements which can capture the decaying foundation deformation away from loading points. The Vlasov model is a two parameter model including a modulus of subgrade reaction similar to the Winkler model, and a shear coefficient. In this model, subgrade reaction pressure, q , is related to surface deflection, w , as follows:

$$q = kw - G\nabla^2 w \quad (2.4)$$

where k is the modulus of subgrade reaction, G is a coefficient describing the shear interaction between adjacent springs, and ∇^2 is the Laplacian operator [6, 7, 10, 17, 23, 29]. To visualize this model, a combination of a shear layer resting on top of the spring layer can be used as shown in Figure 2.3.

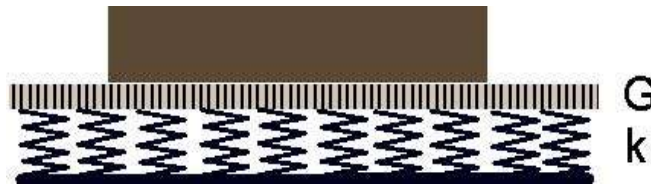


Figure 2.3 Slab on Pasternak foundation [6]

The soil deflection, away from the point of application of the load, decays faster than what the Boussinesq model predicts. The Pasternak foundation prediction for deflection decay is much faster than the Boussinesq, and it is a better approximation of actual foundation deflections. By comparing the Winkler and the Pasternak models, Pronk [18] suggests that Pasternak model is a logical improvement of the Winkler model as corroborated by the experiments of Ioannides et al. [10]. After all, in the Vlasov model, if G is set to zero, the foundation will reduce to Winkler foundation [6, 7, 10, 18]. ILLI-SLAB was the first finite element software to implement the slab on the Pasternak foundation. The studies of Ioannides et al. show that the flexural rigidity of the plate affects Vlasov's parameters and thus the definition of the two parameters is not unique and not very straightforward to estimate from field data [6, 10].

2.1.4 Kerr Model

The Pasternak model was generalized by Vlasov and Leontev [17], and later expanded by Kerr [23]. Khazanovich and Ioannides [21] proposed a finite element formulation for the soil beyond the slab, which was based on the Vlasov and Leontev assumption. For the soft layer on top of the stiffer subgrade, Vlasov suggested a higher order idealization to get more accurate solutions than Pasternak's model. In this assumption, the deflections beyond the slab are a function of the deflection of the nearest point of the slab edge and the subgrade parameters. These studies resulted in the three-parameter Kerr model. The Kerr model is a combination of the Winkler and the Pasternak models. A plate resting on the Kerr model is shown in Figure 2.4. This model considers a two-layer foundation assuming that the upper layer is very thin so that its shear stiffness is negligible [6, 7, 20].

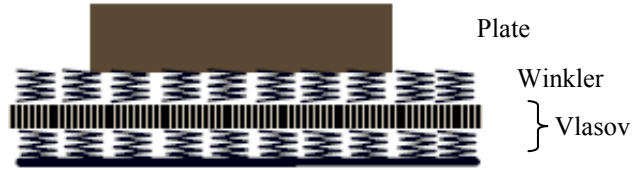


Figure 2.4 Slab on Kerr foundation [6]

Khazanovich and Ioannides [21] showed that if the stiffness of the upper Winkler springs is large enough, the Kerr model results would be the same as with those of the Pasternak model. However, a very high stiffness for upper Winkler springs cause numerical instability and non-convergence of the finite element solution [6, 7, 21, 22]. For high $\frac{K_{pu}}{K_{pl}}$ ratios, the Kerr model

behaves as a Vlasov model, whereas for very low $\frac{K_{pu}}{K_{pl}}$, the Kerr model approximates the

Winkler model [7]. One of the weaknesses of the Kerr model is its requirement of three parameters that are difficult to determine experimentally.

2.1.5 Zhemochkin, Sinitsyn and Shtaerman (ZSS)

Zhemochkin and Sinitsyn in 1947 and then Shtaerman in 1949 proposed another two-parameter subgrade that utilizes plasticity concepts [7]. The Zhemochkin-Sinitsyn-Shtaerman (ZSS) model consists of a series of independent springs on an elastic half-space. The ZSS model is a combination of a Winkler and a Boussinesq model. Non-recoverable spring deformations simulate the plastic component and the resilient parts of soil deflections are modeled through the elastic half-space. For very high k values (Winkler parameter), ZSS produces results similar to the conventional Boussinesq half-space. As plastic deformations usually occur only at the slab edges, Shtaerman and Hemtenyi suggested a simpler linear model by ignoring the plastic deformations and assuming both deflection components as elastic, which is the assumed behavior in the JSLAB implementation [7]. The ZSS subgrade permits a deflection profile discontinuity at a loaded slab edge, which is equivalent to the Winkler model.

2.2 LOAD TRANSFER DEVICES

To allow for slab movements due to temperature and moisture variations, PCC pavements can be constructed with transverse and longitudinal joints. A critical point for maintaining a satisfactory performance of PCC pavements is the transfer of the loads across these joints. Having proper transfer mechanisms will result in smaller deflections and reduced intrusion of water into the joints that leads to a loss of load bearing capacity of the foundation [26, 30].

Both theoretical and field results show that increasing the thickness of the slab or subbase is not a sufficient solution to prevent slab faulting or breaks at the corner of the slab. An adequate load transfer mechanism can prevent large permanent deformations so that slab faulting or breaks at the corner of the slab cannot occur [25].

2.2.1 Aggregate and Key Interlock

Aggregate and key interlock is perceived as the simplest means of load transfer when the crack faces are held together. This mechanism is useful only if the traffic volume is low, and the pavement lay on a firm support such as a stabilized subbase. The aggregate and key interlock mechanisms transfer the loads across cracks or joints only by shear. Figure 2.5 illustrate the application of aggregate interlocks. The material properties of the concrete, such as coarse aggregate type, mix design, and gradation, have a significant impact on the aggregate interlock load transfer [14, 25, 26].



Figure 2.5 Aggregate interlocks [41]

2.2.2 Dowels and Ties

The National Cooperative Highway Research Program (NCHRP) Synthesis 211 states that when slab lengths increase the use of the aggregate and key interlock begins to become ineffective [30]. Many highway agencies utilize dowel/tie bars to interconnect slabs to transfer the edge loading and reduce the differential deflection of the mating slabs; Figure 2.6 shows the implementation of these transfer devices. Dowel bars are then used as structural elements for eliminating or reducing the potential for faulting, pumping and corner breaks [10, 26, 30].



(a) Tie Bars

(b) Dowels

Figure 2.6 Application of dowels and tie bars [41]

CHAPTER 3: THE FINITE ELEMENT CORE PROCESSOR

The MATLAB software was used to develop the new processing core and to implement the required improvements and new capabilities. The decision was based on MATLAB's built-in capabilities to handle matrix and vector operations on which the FEM is based. This section describes the finite element formulation used in the modeling of the slabs, foundation and load transferring devices.

3.1 PAVEMENT SECTION MODELING

Figure 3.1 illustrates the mathematical modeling of a typical jointed-pavement section. To implement the necessary improvements to JSLAB2004, the general geometric modeling of the jointed slabs and foundation was significantly changed. The pavement structure (layers of slabs and soils) are treated as three dimensional. Unbonded slab layers were modeled independently and connected to each other using gap elements. The bottom slab layer and the top foundation layer were also connected thru gap elements. To model the Winkler foundation, the foundation layers below each slab were modeled as disconnected elements to allow for the independence of Winkler "springs" across the joints. To model foundations with shear layer or the Boussinesq foundation, the soil elements were connected across the joints with high stiffness springs. This FE structure deviates from the one used in JSLAB2004 where all slabs and foundation stiffness matrices were condensed to the top slab.

3.1.1 Mindlin Plate Theory

Although JSLAB2004 used the Kirchhoff plate theory that applies to thin to medium-thick plates, for NYSlab the Mindlin plate theory was used to account for the shear deformation that becomes significant for relatively thick plates. In this plate formulation, the rotation of the plate cross section is not equal to the derivatives of the displacement w as is the case in the Kirchhoff plate theory. The cross-section rotations β_x and β_y are thus, independent of the transverse displacement. The governing equations for a single isotropic plate will be discussed first and then an explanation of the treatment of bonded plates (laminates) in NYSlab will be presented.

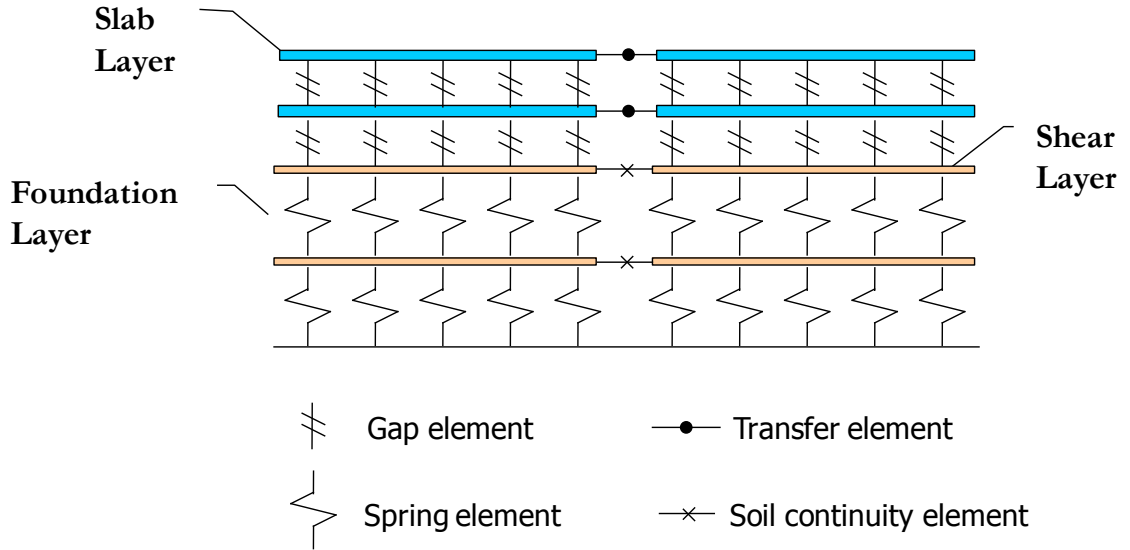


Figure 3.1 Jointed slab pavement section in NYSlab

The displacement and strain equations are [32]:

$$u(x, y, z) = -z\beta_x(x, y) \quad v(x, y, z) = -z\beta_y(x, y) \quad w = w(x, y) \quad (3.1)$$

$$\begin{bmatrix} \varepsilon_{xx} \\ \varepsilon_{yy} \\ \gamma_{xy} \end{bmatrix} = - \begin{bmatrix} \frac{\partial \beta_x}{\partial x} \\ \frac{\partial \beta_y}{\partial y} \\ \frac{\partial \beta_x}{\partial y} + \frac{\partial \beta_y}{\partial x} \end{bmatrix} \quad (3.2a)$$

$$\begin{bmatrix} \gamma_{xz} \\ \gamma_{yz} \end{bmatrix} = \begin{bmatrix} \frac{\partial w}{\partial x} - \beta_x \\ \frac{\partial w}{\partial y} - \beta_y \end{bmatrix} \quad (3.2b)$$

Using a plain stress constitutive matrix for isotropic plates, the strains are related to the stresses as follows:

$$\begin{bmatrix} \sigma_x \\ \sigma_y \\ \tau_{xy} \end{bmatrix} = -z \frac{E}{1-\nu^2} \begin{bmatrix} 1 & \nu & 0 \\ \nu & 1 & 0 \\ 0 & 0 & 1-\nu/2 \end{bmatrix} \begin{bmatrix} \frac{\partial \beta_x}{\partial x} \\ \frac{\partial \beta_y}{\partial y} \\ \frac{\partial \beta_x}{\partial y} + \frac{\partial \beta_y}{\partial x} \end{bmatrix} \quad (3.3a)$$

$$\begin{bmatrix} \tau_{yz} \\ \tau_{zx} \end{bmatrix} = \kappa G \begin{bmatrix} \frac{\partial w}{\partial y} - \beta_y \\ \frac{\partial w}{\partial x} - \beta_x \end{bmatrix} \quad (3.3b)$$

where E is Young's modulus, G is shear modulus, ν is Poisson's ratio and κ is a shear correction factor, to account for the non-uniform distribution of transverse shear stresses over the plate thickness. Since the cross sections of plates are always rectangular, κ was assumed as 5/6 in the transverse shear stress equations [32].

The equilibrium equations are the same as those for the Kirchhoff plate theory, i.e.:

$$\frac{\partial V_x}{\partial x} + \frac{\partial V_y}{\partial y} + q = 0 \quad (3.4a)$$

$$-V_x + \frac{\partial M_x}{\partial x} + \frac{\partial M_{xy}}{\partial y} = 0 \quad (3.4b)$$

$$-V_y + \frac{\partial M_{xy}}{\partial x} + \frac{\partial M_y}{\partial y} = 0 \quad (3.4c)$$

where, V_x , V_y , M_x , M_y , and M_{xy} are shear force and moment intensities. Shear force and moments in matrix form would be represented as follows:

$$\text{Moment-curvature relationships: } \begin{pmatrix} M_x \\ M_y \\ M_{xy} \end{pmatrix} = -D \begin{bmatrix} 1 & \nu & 0 \\ \nu & 1 & 0 \\ 0 & 0 & 1-\nu/2 \end{bmatrix} \begin{bmatrix} \frac{\partial \beta_x}{\partial x} \\ \frac{\partial \beta_y}{\partial y} \\ \frac{\partial \beta_x}{\partial y} + \frac{\partial \beta_y}{\partial x} \end{bmatrix} \Rightarrow M = -DC\psi_b$$

$$\text{Shear-section rotation relationships: } \begin{pmatrix} V_x \\ V_y \end{pmatrix} = \kappa Gh \begin{bmatrix} \frac{\partial w}{\partial x} - \beta_x \\ \frac{\partial w}{\partial y} - \beta_y \end{bmatrix} \Rightarrow V = \kappa Gh \psi_s$$

where, $D = \frac{Eh^3}{12(1-\nu^2)}$ is the bending or flexural rigidity [32].

3.1.2 Mindlin Plate Element

The finite element formulation of the Mindlin plate element requires three interpolation schemes for w , β_x and β_y . Since all three quantities are independent they can be expressed in terms of the element nodal transverse displacements and right-handed rotations as follows [32], letting w [=] Vertical deflection, θ_x [=] Rotation about x-axis $\equiv \beta_y$, and θ_y [=] Rotation about y-axis $\equiv -\beta_x$

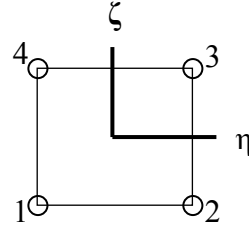
$$w = [N_1 \quad 0 \quad 0 \quad N_2 \quad 0 \quad \dots] \begin{bmatrix} w_1 \\ \theta_{x1} \\ \theta_{y1} \\ w_2 \\ \vdots \end{bmatrix} = N_w^T \mathbf{d} \quad (3.5a)$$

$$\beta_x = [0 \quad 0 \quad -N_1 \quad 0 \quad 0 \quad \dots] \begin{bmatrix} w_1 \\ \theta_{x1} \\ \theta_{y1} \\ w_2 \\ \vdots \end{bmatrix} = N_{\beta_x}^T \mathbf{d} \quad (3.5b)$$

$$\beta_y = [0 \quad N_1 \quad 0 \quad 0 \quad N_2 \quad \dots] \begin{bmatrix} w_1 \\ \theta_{x1} \\ \theta_{y1} \\ w_2 \\ \vdots \end{bmatrix} = N_{\beta_y}^T \mathbf{d} \quad (3.5c)$$

For a four node isoparametric quadrilateral,

$$\begin{pmatrix} N_1 \\ N_2 \\ N_3 \\ N_4 \end{pmatrix} = \begin{pmatrix} \frac{1}{4}(\xi-1)(\eta-1) \\ -\frac{1}{4}(\xi+1)(\eta-1) \\ \frac{1}{4}(\xi+1)(\eta+1) \\ -\frac{1}{4}(\xi-1)(\eta+1) \end{pmatrix} \quad (3.6)$$



The derivatives that appear in the definition of the strains can be defined as:

$$\psi_b = \begin{bmatrix} \frac{\partial \beta_x}{\partial x} \\ \frac{\partial \beta_y}{\partial y} \\ \frac{\partial \beta_x}{\partial y} + \frac{\partial \beta_y}{\partial x} \end{bmatrix} = \begin{bmatrix} 0 & 0 & -\frac{\partial N_1}{\partial x} & 0 & \dots \\ 0 & \frac{\partial N_1}{\partial y} & 0 & 0 & \dots \\ 0 & \frac{\partial N_1}{\partial x} & -\frac{\partial N_1}{\partial y} & 0 & \dots \end{bmatrix} \begin{pmatrix} w_1 \\ \theta_{x1} \\ \theta_{y1} \\ w_2 \\ \vdots \end{pmatrix} \equiv \mathbf{B}_b^T \mathbf{d} \quad (3.7a)$$

$$\psi_s = \begin{bmatrix} \frac{\partial w}{\partial x} - \beta_x \\ \frac{\partial w}{\partial y} - \beta_y \end{bmatrix} = \begin{bmatrix} \frac{\partial N_1}{\partial x} & 0 & N_1 & \frac{\partial N_2}{\partial x} & \dots \\ \frac{\partial N_1}{\partial y} & -N_1 & 0 & \frac{\partial N_2}{\partial y} & \dots \end{bmatrix} \begin{pmatrix} w_1 \\ \theta_{x1} \\ \theta_{y1} \\ w_2 \\ \vdots \end{pmatrix} \equiv \mathbf{B}_s^T \mathbf{d} \quad (3.7b)$$

Without going through the weak formulation of the governing equations, the element stiffness matrix is calculated as follows using numerical integration,

Bending Stiffness Matrix:

$$k_b = \int_{-1}^1 \int_{-1}^1 B_b C B_b^T \det J d\xi d\eta = \sum_{i=1}^m \sum_{j=1}^n w_i w_j B_b(\xi_i, \eta_j) C B_b^T(\xi_i, \eta_j) \det J(\xi_i, \eta_j) \quad (3.8)$$

Shear Stiffness Matrix:

$$k_s = \kappa G h \int_{-1}^1 \int_{-1}^1 B_s B_s^T \det J d\xi d\eta = \kappa G h \sum_{i=1}^m \sum_{j=1}^n w_i w_j B_s(\xi_i, \eta_j) B_s^T(\xi_i, \eta_j) \det J(\xi_i, \eta_j) \quad (3.9)$$

Total Stiffness Matrix: = $k_b + k_s$

where

$$C = \frac{Eh^3}{12(1-\nu^2)} \begin{bmatrix} 1 & \nu & 0 \\ \nu & 1 & 0 \\ 0 & 0 & 1-\nu/2 \end{bmatrix}; \quad G = E/2(1-\nu); \quad \kappa = 5/6; \quad (3.10)$$

The plate element equations described above suffers from “shear locking” when the thickness becomes small and the shear term becomes dominant. Several numerical schemes have been implemented to solve this problem. Selective reduced integration where the shear stiffness matrix is calculated using one quadrature point while the bending stiffness is calculated using four is one of these methods [32]. Although reduced integration eliminates the shear locking problem, it produces the problem of rank deficiency which can lead to oscillatory behavior. Bathe and Dvorkin [33] described an effective element which does not lock in thin plate/shell analysis and does not have any spurious zero energy modes [33]. This element, which is commonly called MITC, is used in NYSlab. In this element formulation, the interpolation functions used to determine the shear strains are defined as follows in the natural space:

$$\begin{aligned} \gamma_{\xi\xi} &= \frac{1}{2}(1+\eta)\gamma_{\xi\xi}^A + \frac{1}{2}(1-\eta)\gamma_{\xi\xi}^C \\ \gamma_{\eta\xi} &= \frac{1}{2}(1+\xi)\gamma_{\eta\xi}^D + \frac{1}{2}(1-\xi)\gamma_{\eta\xi}^E \end{aligned} \quad (3.11)$$

where $\gamma_{\xi\xi}^A$, $\gamma_{\xi\xi}^B$, $\gamma_{\xi\xi}^C$ and $\gamma_{\xi\xi}^D$ are the transverse shear strains at points A, B, C and D located at the midpoints of the sides of the quadrilateral element (see Figure 3.2). These are called “tying” points and is where the isoparametric interpolations predict exact strains. Thus, the MITC interpolation uses the strains at the tying points to extrapolate the strains using a linear interpolation. This translates into a reduction of the order of the interpolation functions from bi-linear to linear.

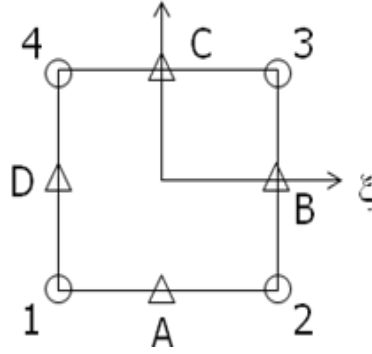


Figure 3.2 Quadrilateral elements with MITC tying points

This reduction of order of interpolation from bi-linear to linear of the shear strain components produces a stiffness matrix that has very good convergence characteristics for any plate thickness. The shear stiffness matrix in this formulation is integrated using four quadrature points.

3.1.3 Foundation Elements

All the foundation models, except for the solid elastic, can be model as a single or a combination of two Vlasov layers in series. For example the Kerr foundation can be modeled as two Vlasov layers where the shear parameter on the top layer is set to zero. The Winkler foundation is modeled as one Vlasov layer with a zero shear parameter and the ZSS foundation is modeled as a Vlasov layer with zero shear coefficients on top of a solid elastic (Boussinesq) foundation. If several foundation layers across the pavement section need to be modeled, the entire foundation then becomes a series of Vlasov layers with the appropriate parameters. The solid elastic foundation can only appear at the bottom of the pavement section as part of a ZSS layer or as the only foundation layer.

In NYSlab the Vlasov element is modeled as an eight node element with one degree of freedom per node associated with the vertical displacement. The Winkler contribution to the stiffness matrix for this element is calculated as follows,

$$k_{w1} = k \iint_A B_w B_w^T dA \quad (3.12)$$

where

$$B_w = [N_1 \ 0 \ 0 \ N_2 \ 0 \ \dots] \quad (3.13)$$

k is the modulus of subgrade reaction and the shape functions are the same isoparametric interpolation functions used for the plate element discussed in the previous section.

The integration indicated to calculate k_{w1} is over a horizontal cross section of the element. The total element Winkler stiffness matrix is then calculated as:

$$k_w = \begin{bmatrix} k_{w1} & -k_{w1} \\ -k_{w1} & k_{w1} \end{bmatrix}_{8 \times 8} \quad (3.14)$$

The shear layer contribution to the stiffness matrix is calculated from:

$$k_{vs} = G \iint_A \mathbf{B}_{vs} \mathbf{B}_{vs}^T dA$$

where

$$\mathbf{B}_{vs}^T = \begin{bmatrix} \frac{\partial N_1}{\partial x} & 0 & 0 & \frac{\partial N_2}{\partial x} & \dots \\ \frac{\partial N_1}{\partial y} & 0 & 0 & \frac{\partial N_2}{\partial y} & \dots \end{bmatrix} \quad (3.15)$$

G is the shear parameter and the shape functions the isoparametric functions previously discussed.

The total Vlasov element stiffness matrix is then the sum of the two stiffness matrices as follows,

$$k_{Vlasov} = \begin{bmatrix} k_{w1} + k_{vs} & -k_{w1} \\ -k_{w1} & k_{w1} \end{bmatrix}_{8 \times 8} \quad (3.16)$$

The solid elastic (Boussinesq) foundation model is not based on a FEM formulation but uses a flexibility matrix that then is inverted to obtain a stiffness matrix. The flexibility matrix is calculated as follows,

$$S_{ij} = \frac{(1-\nu_f^2)}{\pi E_f r_{ij}} \quad (3.17)$$

where S_{ij} is the deflection at node i caused by a unit force at node j , and r_{ij} is the distance between nodes i and j .

$$S_{ii} = \frac{(1-\nu_f^2)}{ab\pi E_f} \frac{1}{2} (b \ln((a + (a^2 + b^2)^{1/2})/b) + a \ln((b + (a^2 + b^2)^{1/2})/a)) \quad (3.18)$$

where S_{ii} is the deflection at node i caused by a unit load at node i . In this equation, a and b are the dimensions of the rectangular element formed by connecting the center points of the four elements connected to each node in the FE mesh of the foundation. For edge and corner nodes this equation is adjusted to account for the fact that there could only be two or one element connected to a node. It should be noted that this formulation is only valid for rectangular elements.

The stiffness matrix of the Boussinesq foundations is then calculated as:

$$K_b = S^{-1} \quad (3.19)$$

This matrix is then added, through a degree of freedom mapping scheme, to the global stiffness matrix.

It is important to note that the flexibility and stiffness matrices of the Boussinesq model are full matrices and thus very memory intensive. This not only affects memory requirements but also increases the computation time for the manipulation of the global stiffness matrix and the solution for the displacement vector.

To reduce the memory and CPU time overhead, the stiffness matrix is made sparse by zeroing all off-diagonal elements associated with nodes separated by more than a specified distance. This distance is an input parameter, but 10 ft was found to produce good results since at that distance the flexibility has decayed significantly. The use of smaller distances tends to significantly affect the stresses in the slabs.

3.1.4 Load Transfer Elements

Adjacent slabs might be connected (jointed) through dowels, ties, aggregate interlock or keyed. Any combination of all or some of these “load transfer” mechanisms can be used in a jointed pavement. Dowels and ties are modeled as beam elements with two degrees of freedom per node including a displacement w and a θ rotation about the axis perpendicular to the beam longitudinal axis (see Figure 3.3). Because of the unconstrained length of the beams is governed by the small separation of the slabs (usually a fraction of an inch), shear deformation cannot be ignored. For this reason a Timoshenko beam is used for the modeling of dowels and ties. Having $\phi = \frac{12EI}{GAL^2}$ as a dimensionless coefficient, the stiffness matrix for the Timoshenko beam is given by the following equation,

$$k_{es} = \frac{EI}{L(1+\phi)} \begin{bmatrix} 12/L^2 & 6/L & -12/L^2 & 6/L \\ 6/L & 4+\phi & -6/L & 1-\phi \\ -12/L^2 & -6/L & 12/L^2 & -6/L \\ 6/L & 2-\phi & -6/L & 4+\phi \end{bmatrix} \quad (3.20)$$

For the aggregate interlock and keyed connection, a bar element with one degree of freedom per node, associated with the longitudinal displacement w , is used. These bars connect corresponding nodes across the jointed slabs. The stiffness of this bar element is calculated from the stiffness per unit length of the interlock or key. The stiffness of this bar element is given by,

$$[k] = EA \int_0^L \begin{bmatrix} \frac{1}{L^2} & -\frac{1}{L^2} \\ -\frac{1}{L^2} & \frac{1}{L^2} \end{bmatrix} dx = \frac{EA}{L} \begin{bmatrix} 1 & -1 \\ -1 & 1 \end{bmatrix} \quad (3.21)$$

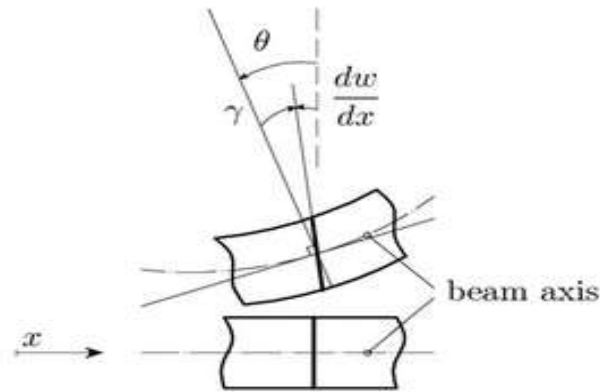


Figure 3.3 Dowel bar Degree of Freedom

3.1.5 Gap Element

Gap elements are used to model the contact between unbounded slab layers and between the bottom slab and the foundation. These elements are modeled as bar elements with one degree of freedom per node and are activated if the gap closes or deactivated if the gap is opened. When a gap element is activated, its stiffness is given as 1,000 times the maximum of the diagonal of the global stiffness matrix. On the other hand, when a gap element is deactivated, its stiffness is given as 10^{-9} times the minimum of the diagonal of the global stiffness matrix. The contact problem is solved through an iterative process over which gap elements are activated and deactivated until two consecutive iterations produce no change in the state of gap elements [42].

3.2 LOAD VECTORS

Pavements are subject to various types of loading conditions with different levels of intensity over their lives. Loads generated by trucks and thermal gradients across the thickness of the slabs are the loads used in the analysis and design of jointed pavements since they are the most significant. The implementation of these two types of loads will be discussed in this section.

3.2.1 Truck Loads

Truck loads are the main types of loads pavements are subjected to. These loads are transferred through the contact “patch” between the tires and the pavement. The contact patch is assumed to be rectangular. It is also assumed that the load is uniform across the patch. Because the rectangular patch will not necessarily have the same dimensions as the slab elements, and more than likely the patch will span more than one slab element, the tire loads are simulated as an equivalent series of point loads. This eliminates the need to calculate the nodal loads associated with a distributed load that does not cover the entire element. The rectangular tire contact patch is treated as a nine node rectangular element (see Figure 3.4), each tire load can be divided into nine concentrated loads that coincide with the nine nodal points. The intensity of these loads is calculated as:

$$F = \int \int_A q N_w dA \quad (3.22)$$

where the shape functions are for those of the nine node isoparametric elements and q is the tire contact pressure. This integral is calculated using the appropriate quadrature rules for a nine node element.

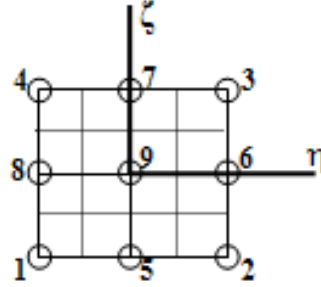


Figure 3.4 Shape Function N_1

The shape (interpolation) functions for the nine node isoparametric element are:

$$\begin{aligned}
 N_1 &= \frac{1}{4}(\xi-1)(\eta-1) - \frac{1}{2}(N_8 + N_5) & N_5 &= \frac{1}{2}(1-\xi^2)(1-\eta) \\
 N_2 &= -\frac{1}{4}(\xi+1)(\eta-1) - \frac{1}{2}(N_5 + N_6) & N_6 &= \frac{1}{2}(1+\xi)(1-\eta^2) \\
 N_3 &= \frac{1}{4}(\xi+1)(\eta+1) - \frac{1}{2}(N_6 + N_7) & N_7 &= \frac{1}{2}(1-\xi^2)(1+\eta) \\
 N_4 &= -\frac{1}{4}(\xi-1)(\eta+1) - \frac{1}{2}(N_7 + N_8) & N_8 &= \frac{1}{2}(1-\xi)(1-\eta^2) \\
 N_9 &= (1-\xi^2)(1-\eta^2)
 \end{aligned} \tag{3.23}$$

3.2.2 Thermal Loads

Changes in temperature could exert additional load to the pavement. During the day the temperature of the top of the slab is higher in comparison with the bottom, causing the slab to curl upward. On the other hand, at night time the lower temperatures at the top of the slab force it to curl downward. To calculate the thermal loads, a thermal gradient given by a cubic function is assumed. This order of polynomial was selected because it is common for temperature to be measured at four points across the thickness of the slabs at pavement test sites. Assuming the origin at the mid-plane of the slab, the temperature gradient is defined as:

$$\Delta t = a_0 + a_1 z + a_2 z^2 + a_3 z^3 \tag{3.24}$$

where the a_i s can be fitted from field data measured at a specific pavement site. The moments caused by the thermal loads can then be calculated as:

$$M_T = D \iint_A C B_b \left[\int_{z_b}^{z_t} \alpha \Delta t z dz \right] dA \tag{3.25}$$

where B_b is as defined in Section 3.1.2, α is the linear coefficient of thermal expansion and z_b and z_t are the distances from the “Neutral Plane” to the bottom and top of the slab. The interior integral can be calculated analytically, but the integral over the area needs to be calculated using Gauss quadrature rules.

If the pavement section is made of bonded layers with different mechanical properties then the thermal moment should be calculated as:

$$M_T = \sum_i^n \left\{ D_i \iint_A C_i B_b \left[\int_{z_b}^{z_t} \alpha_i \Delta t z dz \right] dA \right\} \quad (3.26)$$

where n is the number of slabs that make the bonded pavement section. In this case, subscript i will identify the corresponding mechanical or geometric property of each slab. The function Δt still is assumed to be the temperature change across the bonded pavement section with origin at the “neutral plane”. The neutral plane concept is similar to the neutral axis in beams, but it only “exists” for cases where the Poisons ratios of all bonded slabs are the same.

CHAPTER 4: CONVERGENCE STUDY

In order for NYSlab to be used with confidence, several verification steps were followed to determine that the governing equations that describe the behavior of the jointed slab system have been accurately implemented in the FE model. One of the critical components in the process was to verify that the finite element model converges to a solution as the number of elements used in the space discretization increases [38].

4.1 NUMBER OF ELEMENTS

The number of elements used in a finite element model is one of the parameters that have the most effect on the numerical accuracy of the solution. In general, a more refined mesh results in more numerically-accurate results [38]. However, a finer mesh leads to a longer execution time. A convergence analysis can be carried out to optimize the mesh fineness without incurring on excessive computation time. The results converge when a significant increase in the number of elements produces an insignificant change in a particular response.

NYSlab can generate uniform and non-uniform meshes with any level of refinement as seen in Figure 4.1. The non-uniform mesh is automatically generated in NYSlab by increasing the number of elements in the regions close to the point of application of the truck loads and on the edges of the slab.

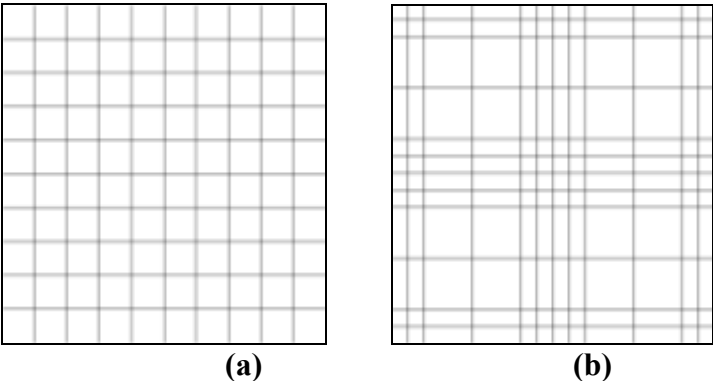


Figure 4.1 Uniform (a) and non-uniform (b) meshes

4.1.1 Single Slab Study

To demonstrate the convergence of the software, a single slab with a single tire load was modeled. The dimensions of the slab were 100 in. by 100 in., which had a 10 in. by 10 in. tire contact at the center with a 100 psi contact pressure. The maximum deflection and normal bending stress were the control parameters used to characterize the convergence.

Figure 4.2 shows the variation in deflection ratio with the number of elements used to model the slab. Deflection ratio is defined as the ratio of the maximum deflection estimated from a given mesh divided by the maximum deflection estimated by a very refined mesh of 128 by 128 elements. The maximum deflection converges very rapidly, for both the uniform and non-uniform meshes. The error is smaller than 2% with only five elements in each direction. A slab with a non-uniform mesh had more concentration of elements near the loaded area and progressively became less refined farther from the load. For example, a slab with 225 elements gave the smallest element size of 1.56 in. under the load, while the largest element was 6.25 in. away from the load (as opposed of uniform element sizes of 6.67 in. for the uniform mesh).

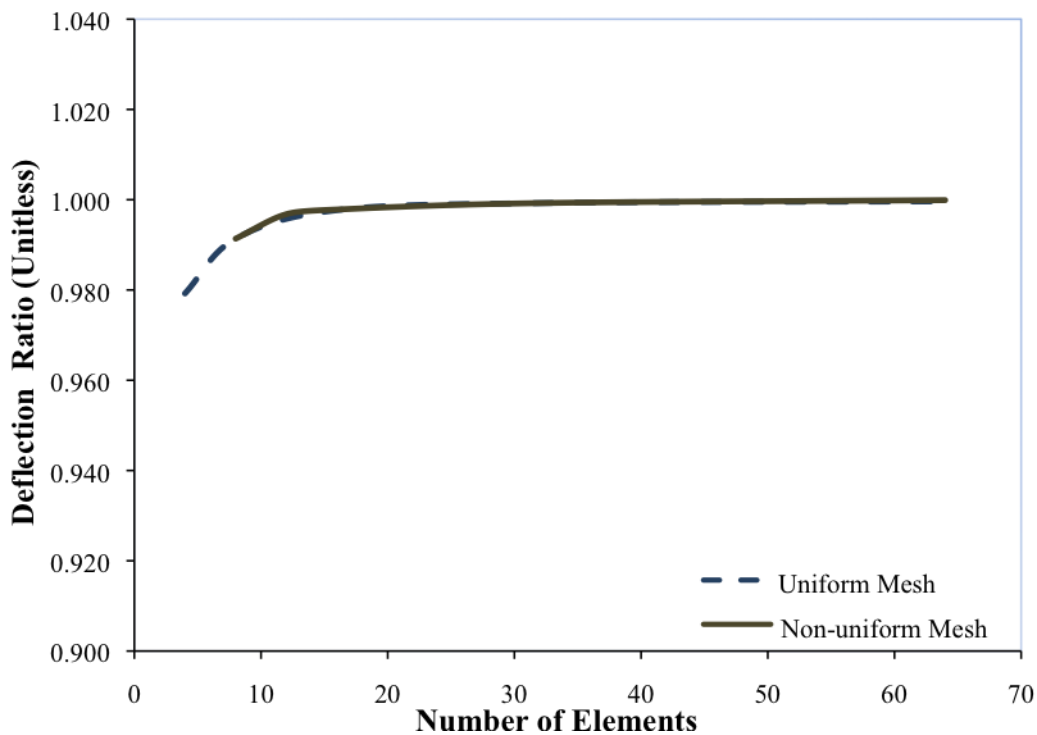


Figure 4.2 Deflections convergences for single slab

The convergence of displacements does not guarantee the convergence of stresses because the stresses are associated with the derivatives of the displacement field. As a result an increase in the number of elements under concentrated loads or close to the boundaries and edges may be required [38]. The stress ratios for uniform and non-uniform meshes as a function of the number of elements are shown in Figure 4.3. Stress ratio is defined as the ratio of the maximum normal

stress estimated from a given mesh divided by the maximum normal stress estimated from a very fine mesh of 128 by 128 elements. Since the slab geometry and the applied load were square in

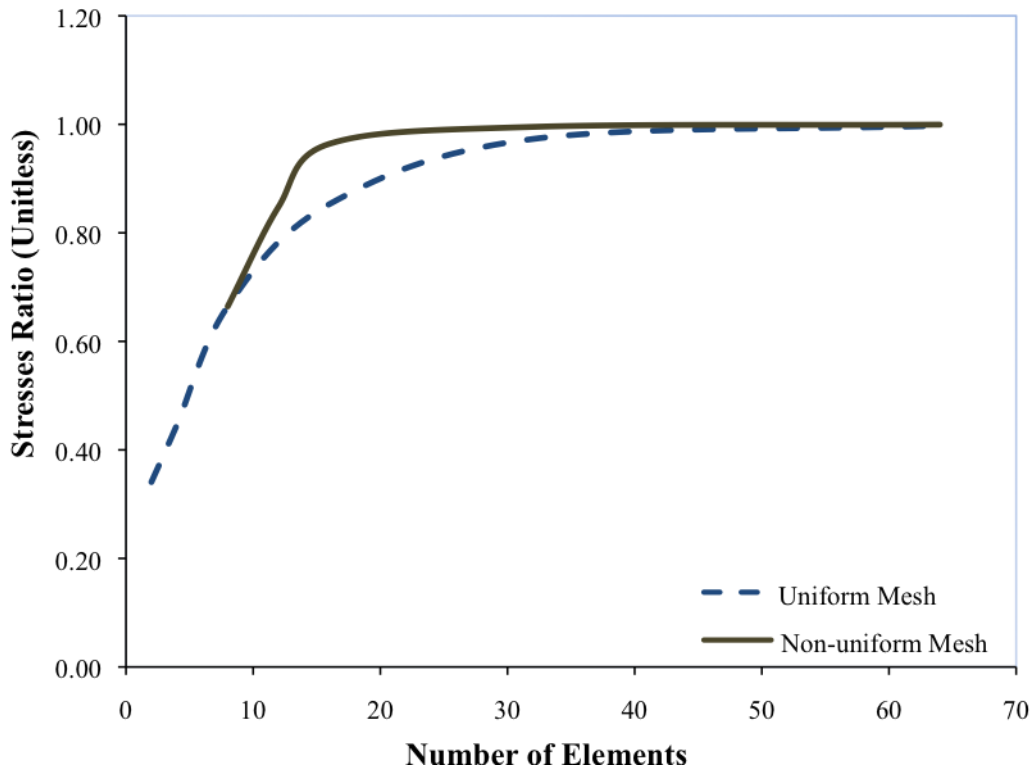


Figure 4.3 Stress convergences for single slab

geometry the stresses in both X and Y directions are the same. The stress converges at a lower rate than displacements, and a finer mesh was needed for the convergence. The stresses converge with a 16 element non-uniform mesh, while uniform mesh needs at least 32 elements in each direction to converge.

4.1.2 Control Case Study

To further evaluate the convergence characteristics of NYSlab, a three by two slab pavement system was used as the control case. The slabs had a dimension of 16 ft by 14 ft. These slabs were loaded with a standard truck shown in Figure 4.4 (called Modified Truck L14 in JSLAB2004 truck library). This truck had a single axle for steering, and two sets of tridem axles. Figure 4.5 shows the truck load layout on the slabs. The front tridem axle of the truck was placed on the center of the second slab in the slow lane. As a result, the last axle of the rear tridem axles could not be fitted within the pavement. For each tire, a contact pressure of 100 psi was applied assuming that the dimensions of the tires were 8 in. by 6 in.

Figures 4.6 through 4.8 show the convergence study for this pavement with a non-uniform mesh. The deflections and stresses are normalized to the results from a case with 40 elements in each direction. As shown in Figure 4.6, the deflections essentially converged with 16 elements in each direction. The largest fluctuation shown in this figure is 0.14%. On the other hand, as

shown in Figures 4.7 and 4.8, the absolute maximum stresses converge with approximately 30 elements in each direction.



Figure 4.4 Scheme of the truck

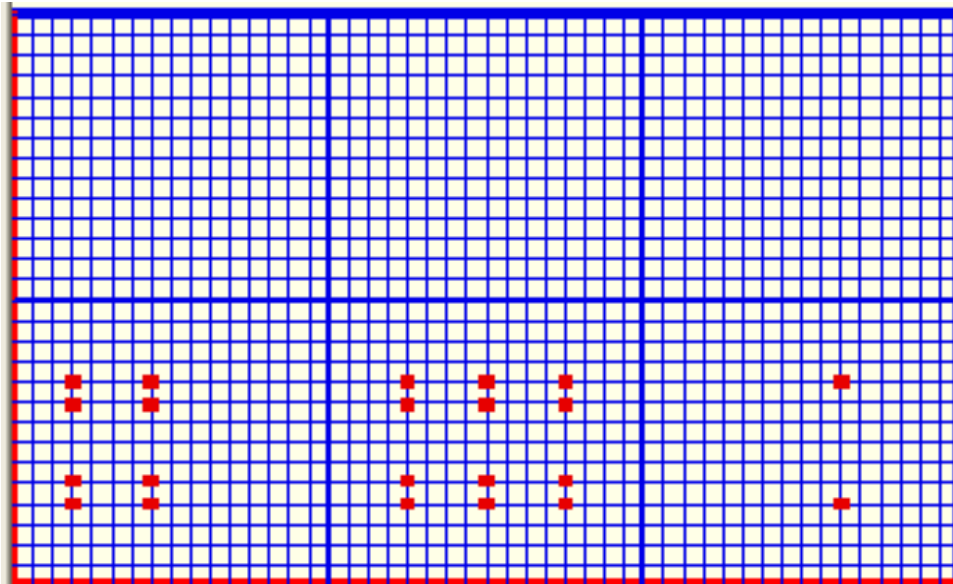


Figure 4.5 Tire layout

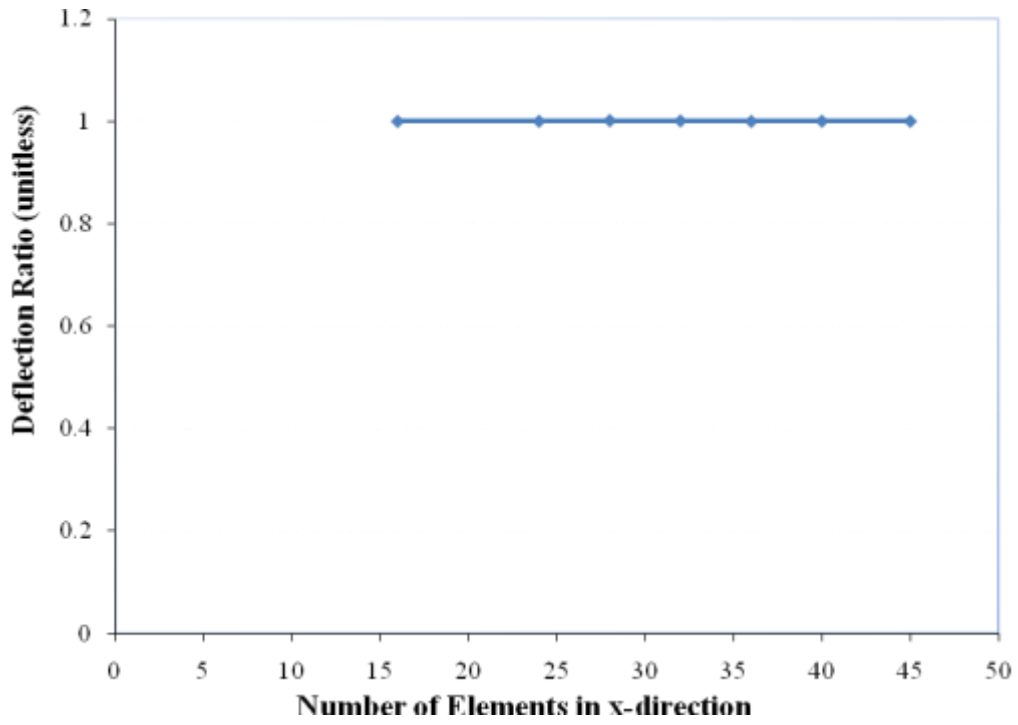


Figure 4.6 Deflections convergences for control case

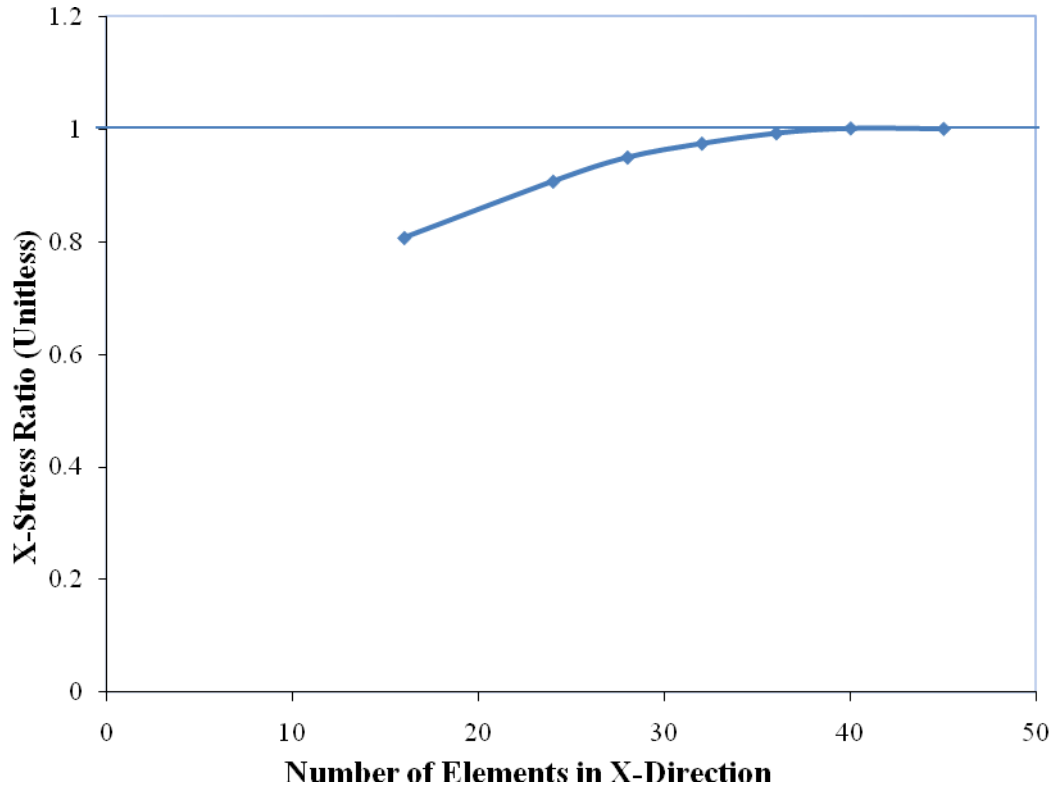


Figure 4.7 Stress convergences in the X direction for control case

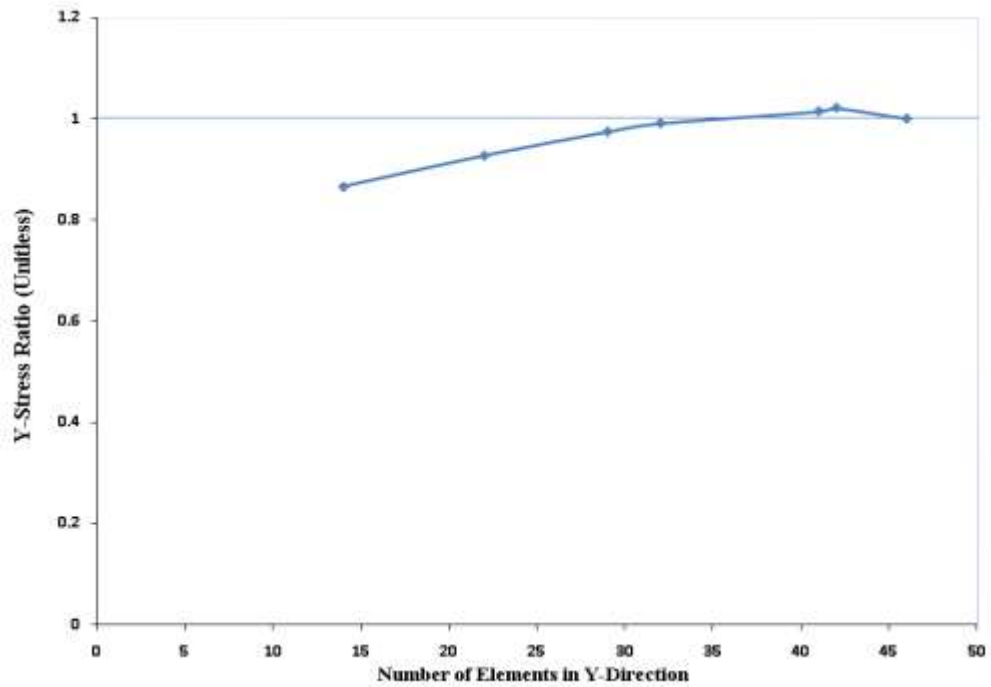


Figure 4.8 Stress convergences in the Y direction for control case

4.2 ELEMENT ASPECT RATIO

The length-to-width ratio of rectangular elements can affect the deflections and stresses. To determine the effect of element aspect ratio, the same single slab with 30 elements in each direction, using uniform mesh was selected to demonstrate this phenomenon. For this study the element aspect ratio was changed while maintaining a constant total number of elements set at 900 (30 square elements in each direction for an aspect ratio of 1). Figures 4.9 and 4.10 represent the results where, a and b are the dimensions of the elements in x (longitudinal) and y (transverse) directions, respectively.

Figure 4.9 shows that the geometry of the element does not have a major effect on the convergence of the absolute maximum deflection. The deflection did not change more than 3% even for a large aspect ratio. As shown in Figure 4.10, the maximum decrease of normal stresses in the x direction is 3.2% relative to square elements, while the maximum stress in the y direction is 9.6% less than the stress for the element with an aspect ratio of one. The reason for the drop in the stress in the y direction is that for large aspect ratios, the number of elements in the y direction decreases below the number required for convergence. Thus, the big error is mostly a result of non convergence and not related to the aspect ratio.

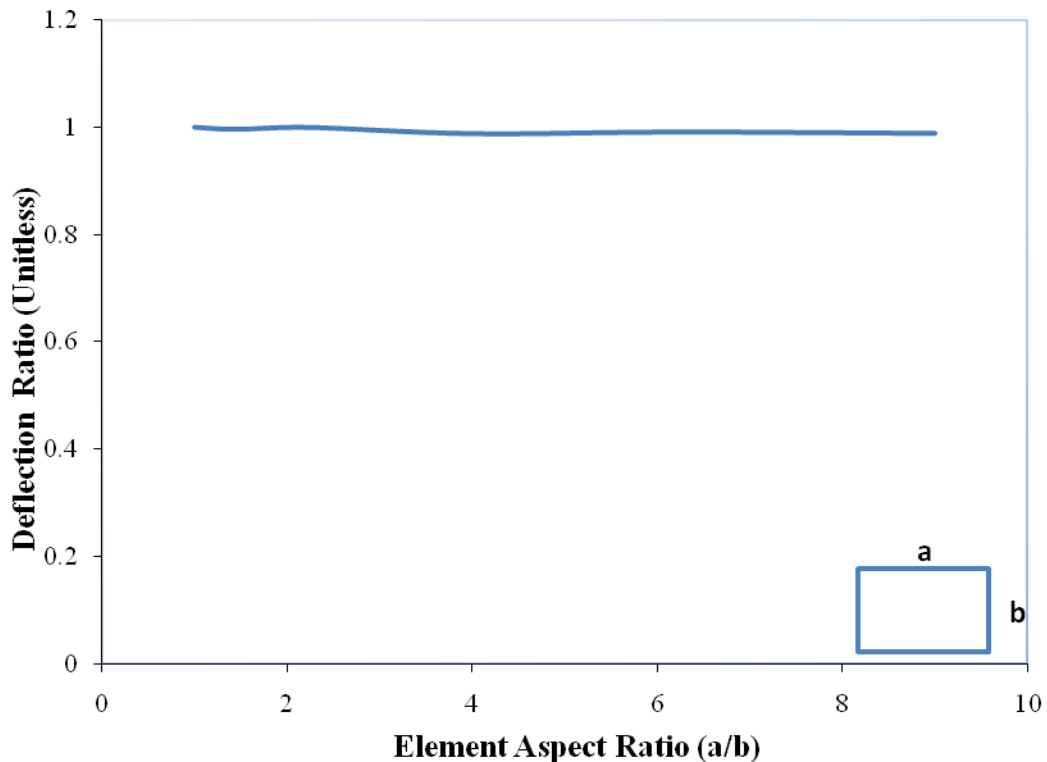


Figure 4.9 Deflections convergence as a function of element aspect-ratio

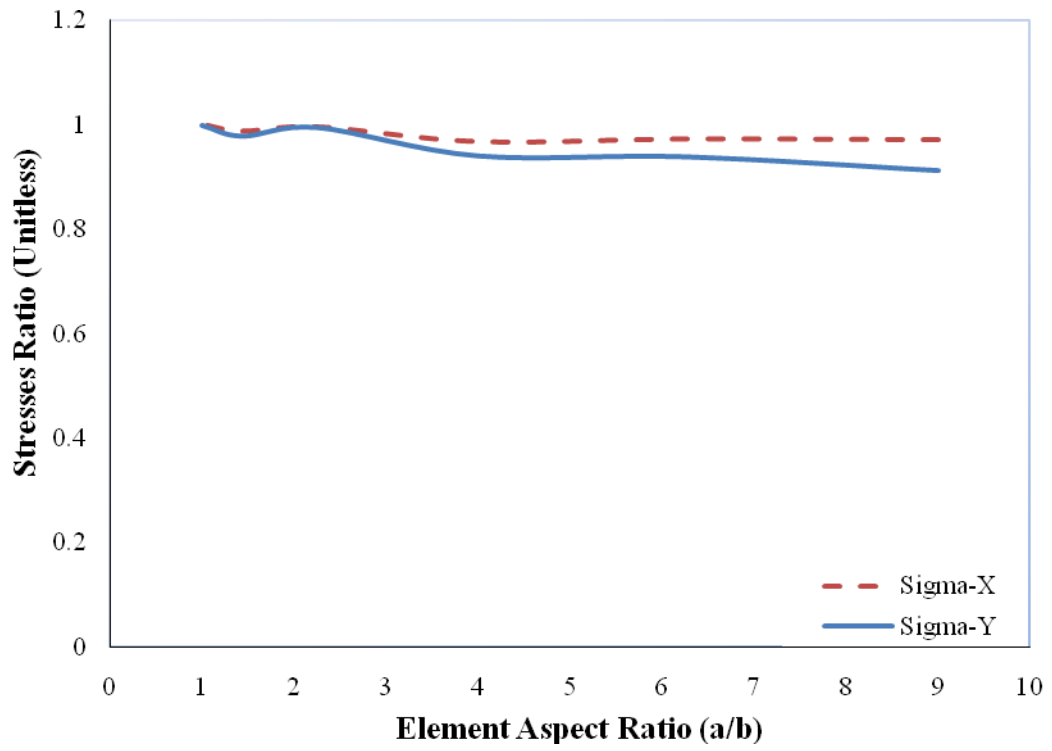


Figure 4.10 Stresses convergence as a function of element aspect-ratio

CHAPTER 5: COMPARISON STUDY

The results from NYSLAB were compared with those from JSLAB2004 and ISLAB2000, using the same pavement geometry and applied loads. The next section will discuss how the comparison case was implemented in each software and the results obtained. The case study is the same one used in Section 4.1.2 and Section 6 below.

5.1 DESCRIPTION OF CASE STUDY

Since JSLAB2004 is restricted to a maximum of three by three slabs with up to two PCC layers, a pavement with three by two slabs was modeled to carry the load of a standard truck. The slabs had a dimension of 16 ft by 14 ft, with a thickness of 12 in. A modulus of elasticity of 4000 ksi, a Poisson ratio of 0.15, and unit weight of 150 pcf were used for the PCC slabs.

ISLAB2000 is capable of analyzing pavements with fine, medium, or coarse meshes. A model with a medium mesh has one element/ft, the fine mesh has two elements/ft, and the coarse mesh has elements that are 2-ft long. In this case study a medium mesh was used to analyze the model for all three software.

The gap between two adjacent slabs was set to 0.25 in. in both directions. The slabs were connected by load transfer devices. The key joints were used in both directions as the common load transfer devices. However, dowels were used for the transfer joints while the tie bars were applied to the longitudinal joints. The stiffness of the key joints in both directions was set to 60,000 psi/in. along the length of the joints. The following material and geometry properties were chosen to model the dowels and tie bars:

Modulus of elasticity (E) = 29,000 ksi
Poisson ratio (ν) = 0.3,
Dowel-Concrete Interaction (DCI) = 1.5×10^6 (lb/in.),
Length of dowel/tie bar in concrete (L) = 9 in.,
Dowels outside diameter = 1.25 in.,
Tie Bar outside diameter = 0.75 in.

The dowels were uniformly distributed in the transfer joints with a 1-ft spacing in the transverse direction and the spacing between the tie bars was set to 2 ft in the longitudinal direction.

ISLAB2000 is capable of analyzing Winkler, Kerr, and Vlasov types of foundations, while JSLAB2004 works properly for Winkler and Vlasov foundations. In this case study, the Winkler foundation with a modulus of subgrade reaction of 200 psi/in was used.

The modified truck, L14 (see Figure 4.4) was selected from the JSLAB2004 library. Figure 5.1 shows the tire dimensions and spacing between the axles of L14 truck in JSLAB2004. The front tridem axle of the truck was placed on the center of the second slab in the slow lane. Since JSLAB2004 is not capable of analyzing the tires located outside of the pavement, the last axle was removed for the JSLAB2004 executions. As mentioned in Chapter 4, 8 in. by 6 in. tires with a contact pressure of 100 psi were used in all programs. In ISLAB2000 an aspect ratio of 0.75 (6/8) was selected for the tire contact for best match with the other two programs.

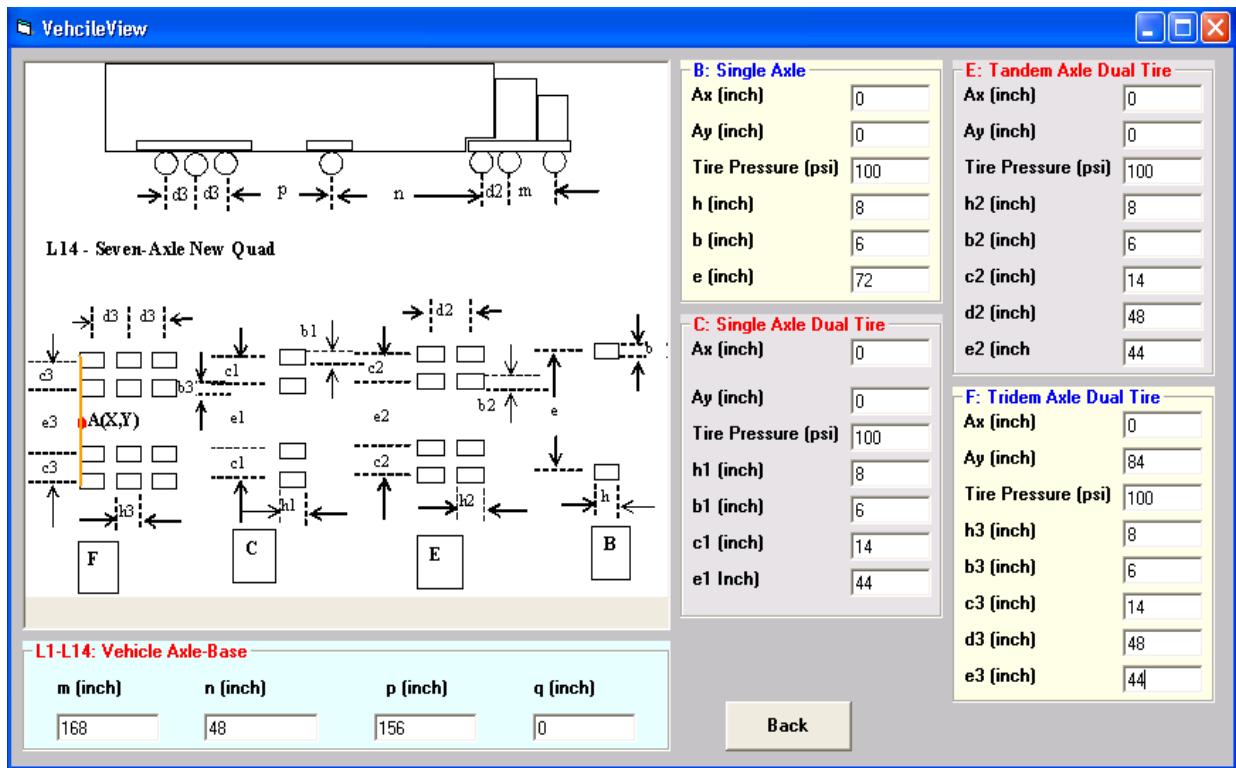


Figure 5.1 Truck dimensions

The reference coordinate system used in ISLAB2000 is not the same as the one used in NYSlab and JSLAB2004. While NYSlab and JSLAB2004 use a right-handed system, ISLAB2000 uses a left-handed system; this means that the normal stress in the x direction in ISLAB2000 corresponds to the normal stress in the y direction in NYSlab. In this study the results are compared using the right-handed system.

Figures 5.2 through 5.4 show the results for JSLAB2004, ISLAB2000, and NYSLAB, respectively. ISLAB2000 and NYSLAB provide contour plots of the results, while JSLAB2004 provides 2D plots of the results.

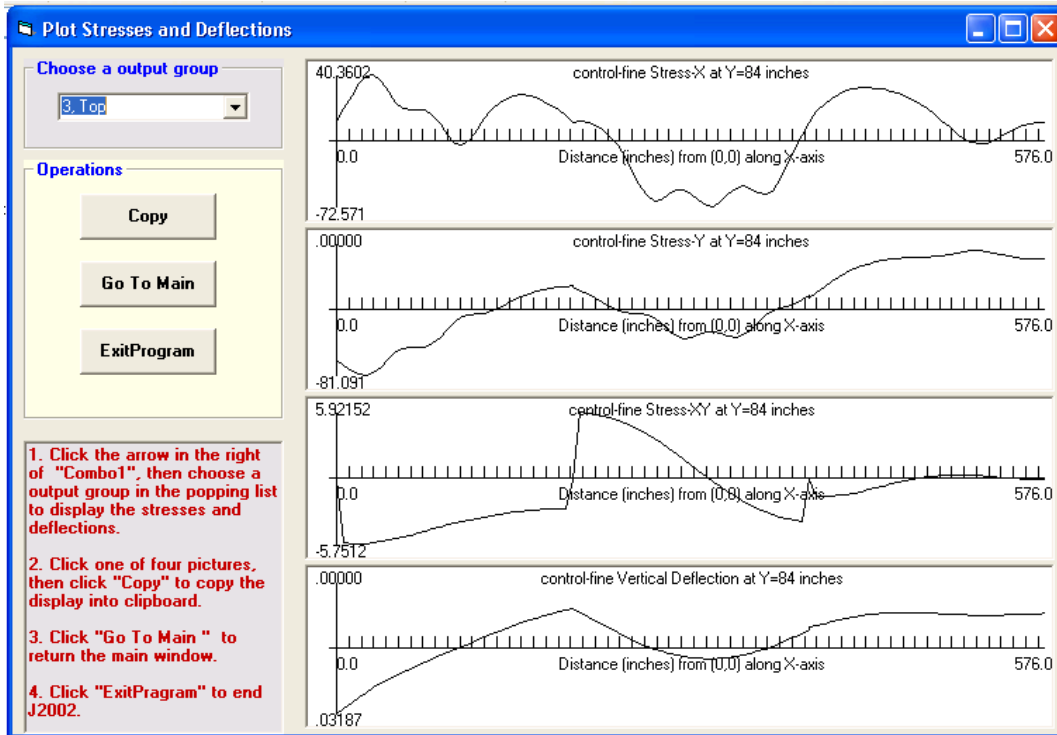


Figure 5.2 JSLAB2004 outputs

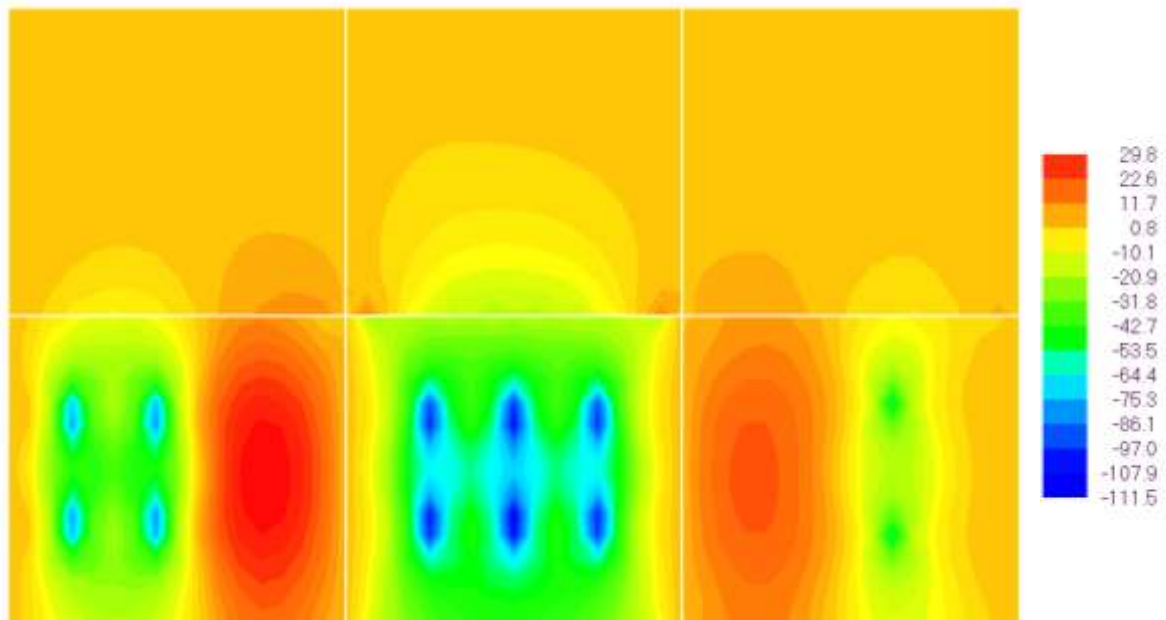


Figure 5.3 ISLAB2000 output (X-stress)

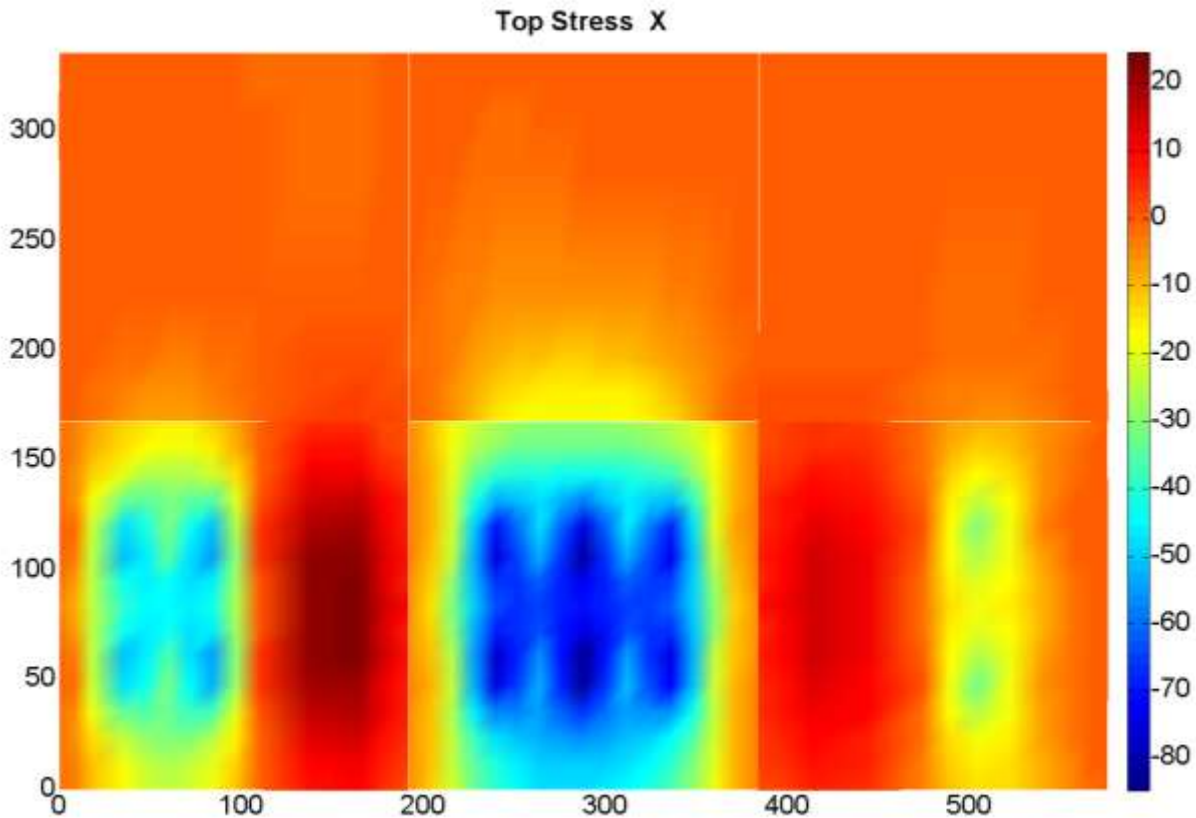


Figure 5.4 NYSLAB MATLAB code output (X- Stress)

5.2 COMPARISON

Figure 5.5 compares deflections along the exterior tires on the pavement from the three programs. The NYSlab and JSLAB2004 deflections are similar while ISLAB2000 exhibits less deflection but with a similar shape to the other programs. The reason for the smaller deflection in ISLAB 2000 is that it subtracts the deformations caused by the self weight of the slab(s).

The stresses in the longitudinal direction along the exterior tires are compared in Figure 5.6. Generally good agreement is observed among the three programs. As reflected in Figure 5.7, the stresses in the transverse direction from the three software packages are very similar, except close to the joints. This can be due to the fact that dowels are modeled differently in NYSlab (see Chapter 3) and/or because the type of the elements is not the same in NYSlab as in the other two codes. NYSlab uses four-node bi-linear isoparametric elements, while the other two codes use a four-node quadratic rectangular element. This should be a topic of further study.

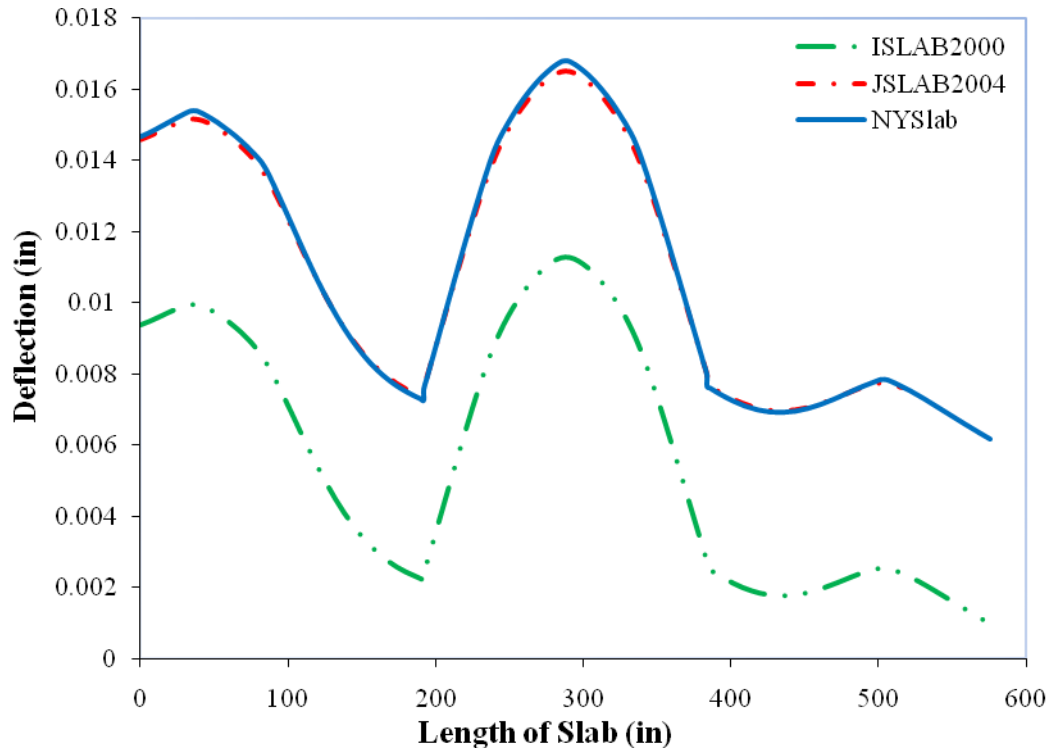
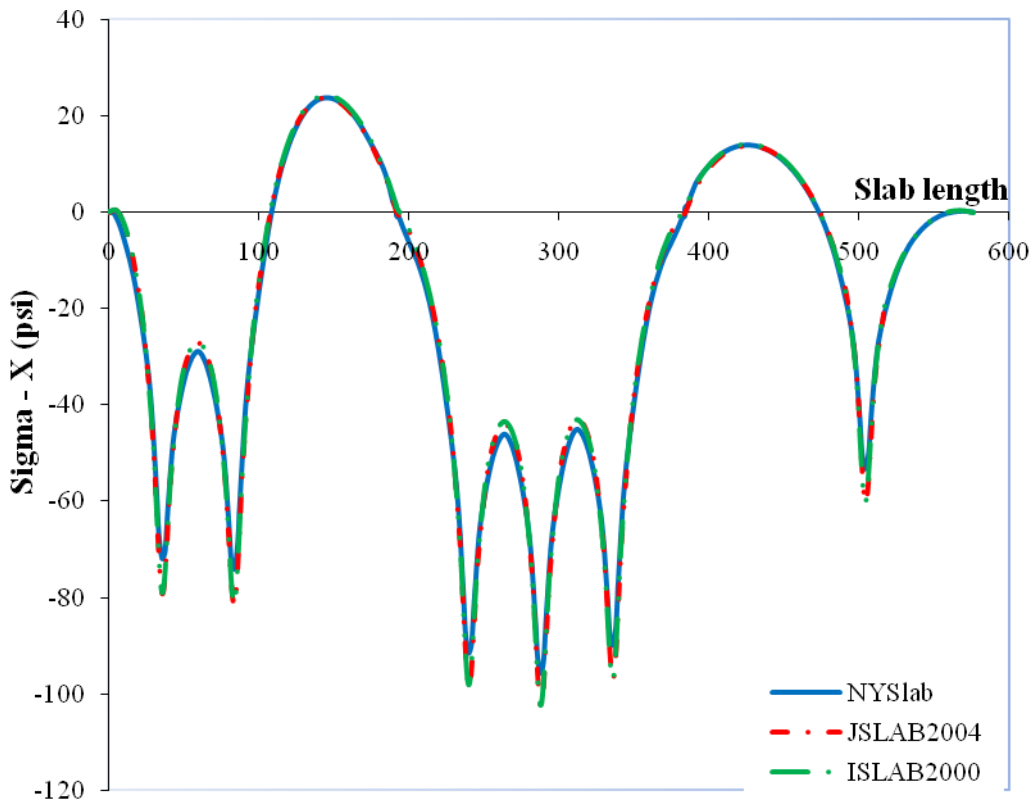


Figure 5.5 Deflections comparison



5.6 Comparisons of stresses in the X direction

Figure

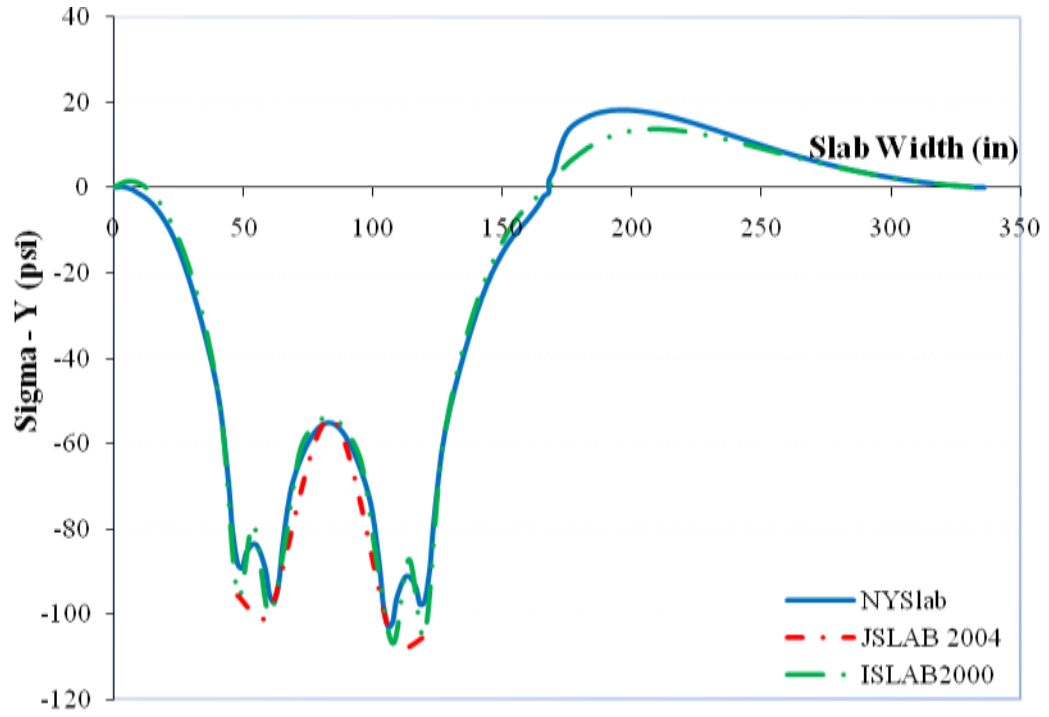


Figure 5.7 Comparisons of stresses in the Y direction

CHAPTER 6: PARAMETRIC STUDY

A series of parametric studies was conducted to better understand the interplay between the most relevant parameters that govern the performance of jointed rigid pavements. The parameters selected for the analysis were the foundation parameters, foundation types, dimension of slabs, the number of slab layers, and temperature gradient. To study the effects of each parameter individually, the relevant targeted parameter was varied, while all other parameters were kept constant. The control model described in detail in the previous chapter was used as the baseline case. A standard truck loading a three by two slab pavement system, the front tridem axle of the truck was placed on the center of the second slab in the slow lane.

6.1 FOUNDATION PARAMETERS

The Winkler, Vlasov and Solid Elastic foundation models were selected for this study. Each model was analyzed by varying the parameters that defined the behavior of the foundation and by calculating the maximum slab stresses and deflections.

6.1.1 Winkler Foundation

The only parameter that defines a Winkler foundation is the modulus of subgrade reaction. The modulus was varied from 50 to 1,000 psi/in and the maximum deflection and bending stresses in the slab were calculated. Figure 6.1 and Figure 6.2 show the variation of the deflection and the stresses in the x and y directions as a function of the modulus of subgrade reaction, respectively. As expected, increasing the modulus of subgrade reaction reduces the maximum deflection and bending stresses. The deflection slope is large when the modulus is small but becomes asymptotic to zero as the modulus increases. Of course the behavior of the deflections and stresses is not only a function of the modulus but also of the geometry and properties of the concrete slab and thus general conclusions cannot be stated. Still, the trend is consistent with expected behavior.

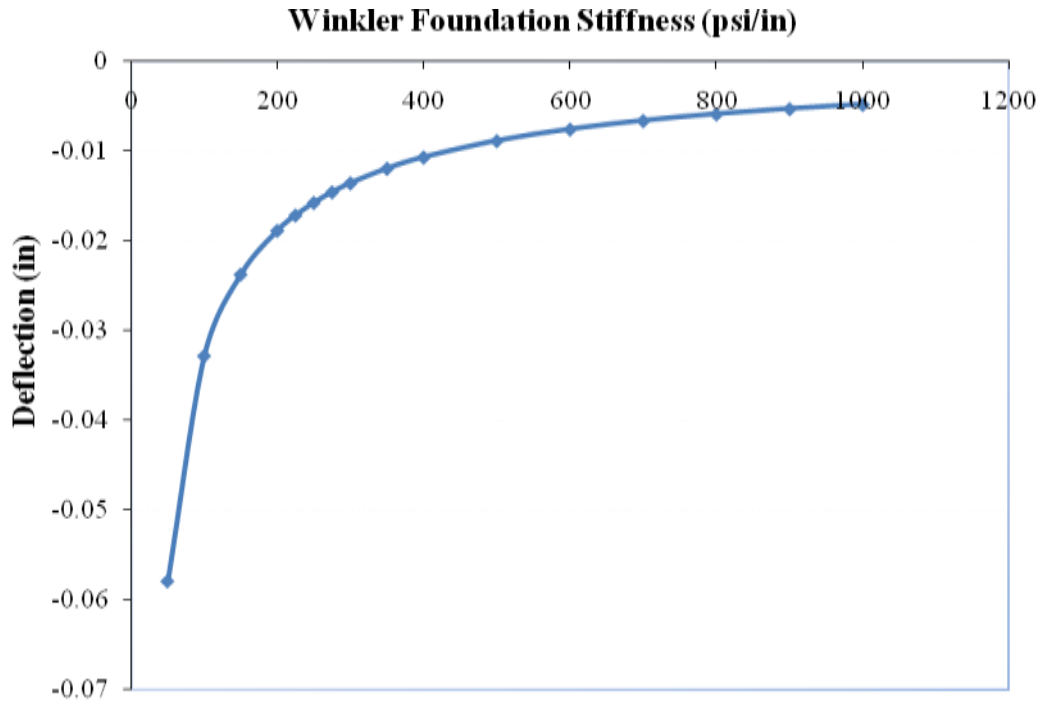


Figure 6.1 Maximum deflection as a function of modulus of sub-grade reaction

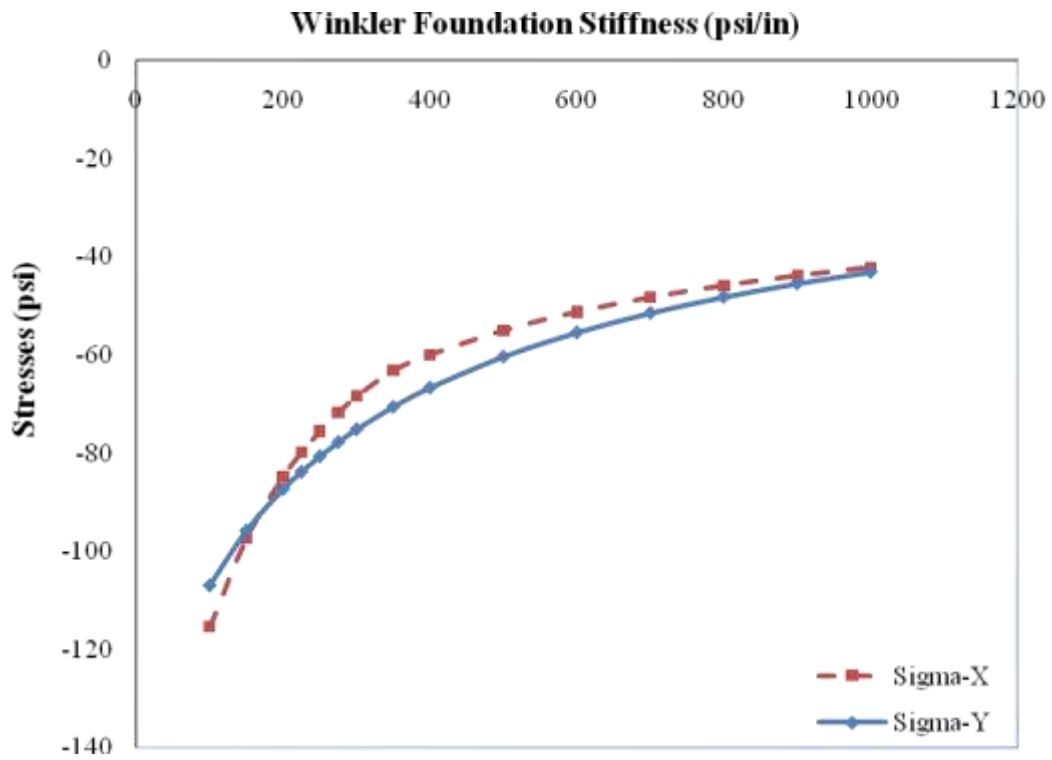


Figure 6.2 Maximum bending stresses as a function of sub-grade reaction

6.1.2 Vlasov Foundation

The Vlasov foundation model behavior is governed by the shear modulus that allows for the modeling of the deflection beyond the point of application of the load. In addition, a modulus similar to the modulus of subgrade reaction in the Winkler model governs the vertical stiffness of the foundation. For this parametric study, the shear modulus was varied from 5 to 120 k/in. and the modulus of subgrade reaction was assumed at 50, 200 and 800 psi/in. Figures 6.3 through 6.5 show the variation of the maximum deflection and stresses as functions of shear modulus (G) and modulus of subgrade reaction (k). As the modulus of subgrade reaction increases, not only the slab deflections and stresses become smaller but they are also less impacted by the shear modulus of the Vlasov foundation. Figure 6.3 shows that for a soft subgrade ($k = 50$ psi/in.), the deflection changes significantly with shear modulus up to a shear modulus of 60 kip/in., beyond which the deflections are almost independent of the shear modulus. The stresses show a similar pattern in Figures 6.4 and 6.5 where the effect of the shear modulus decreases as the modulus of subgrade reaction increases.

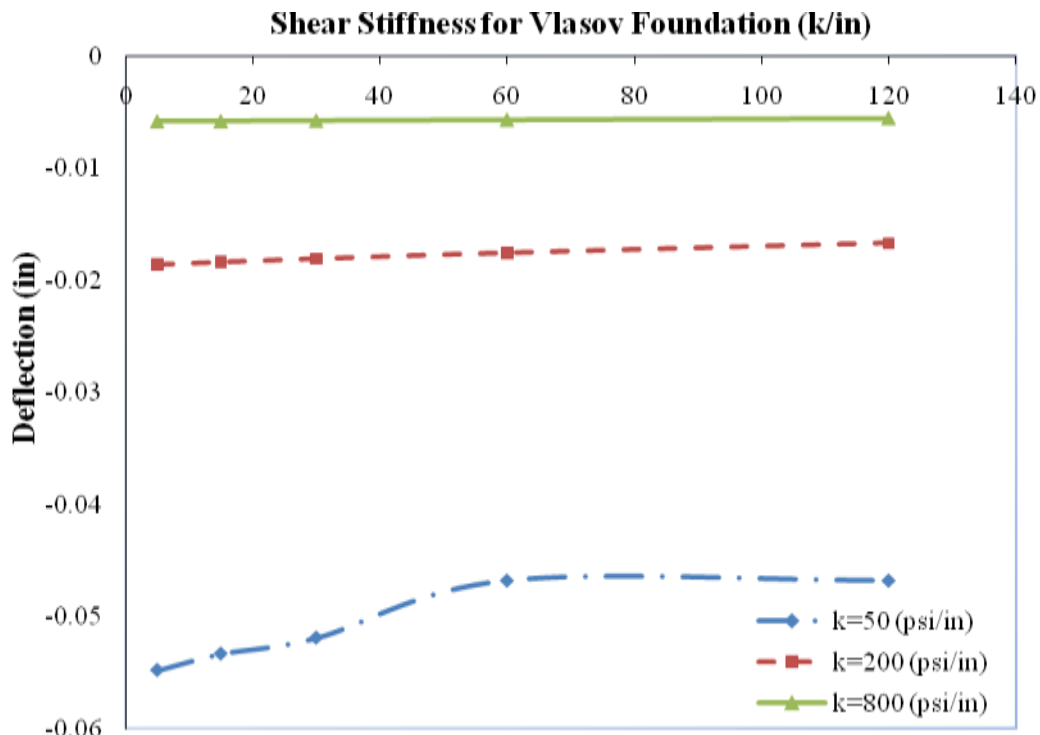


Figure 6.3 Deflection as a function of Vlasov parameters (k,G)

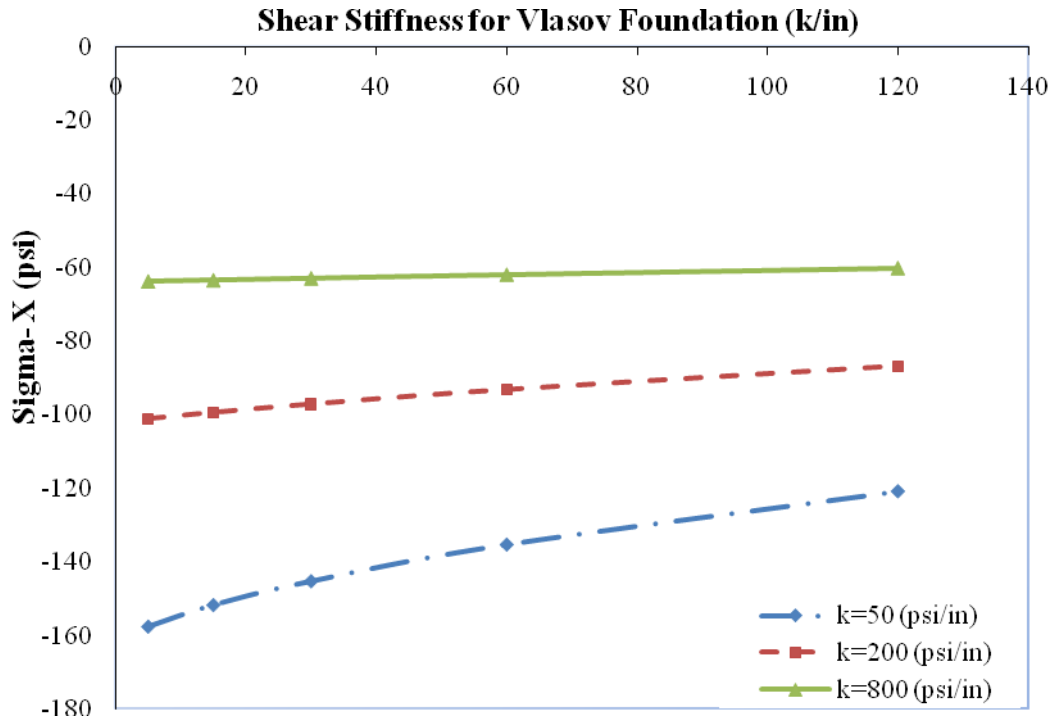


Figure 6.4 Longitudinal stress in the X direction as a function of Vlasov parameters (k,G)

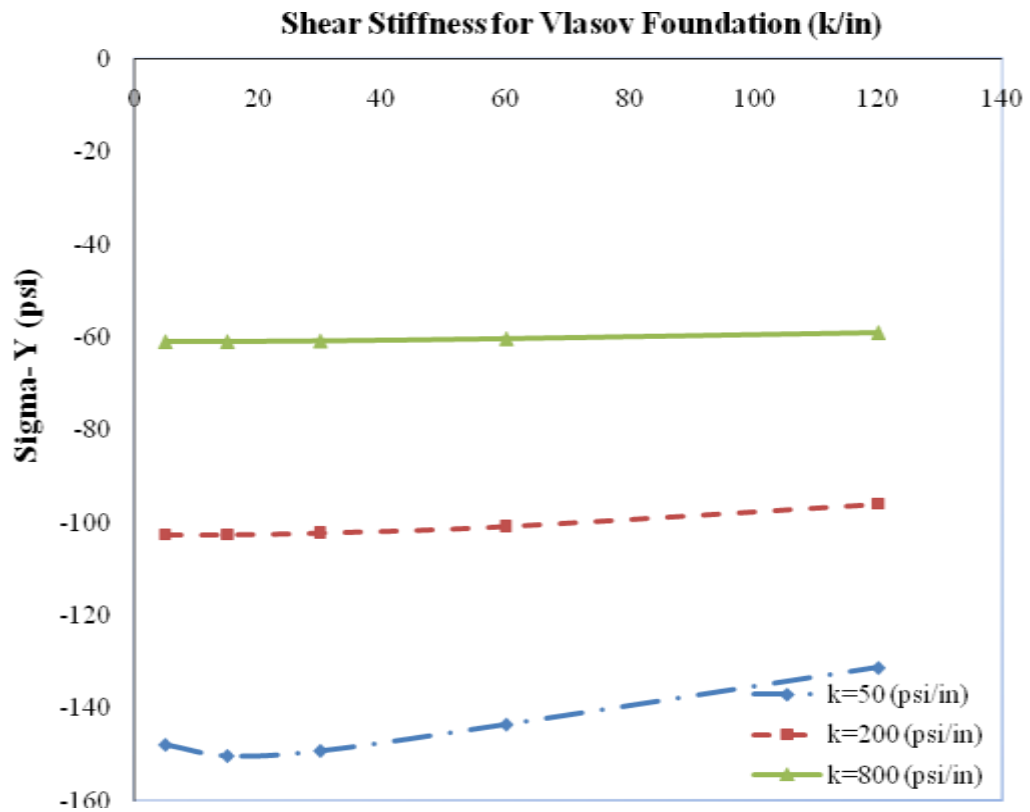


Figure 6.5 Longitudinal stress in the Y direction as a function of Vlasov parameters (k,G)

6.1.3 Solid Elastic Foundation

The solid-elastic (Boussinesq) foundation has two parameters, the modulus of elasticity and the Poisson's ratio. The impact of the modulus of elasticity of the Boussinesq foundation on the maximum deformations and stresses of the slabs for two different Poisson ratios ($\nu=0.3$ and 0.45) is presented in Figures 6.6 through 6.8. Variations in the maximum deflection and stresses are consistent with their inverse relation to the foundation modulus of elasticity. These figures also show that the influence of Poisson's ratio on the deflection and stresses is small. By changing the Poisson ratio from 0.3 to 0.45 (an increase of 50%), the maximum stresses decreased by less than 6% while the maximum deflections decreased by 11% .

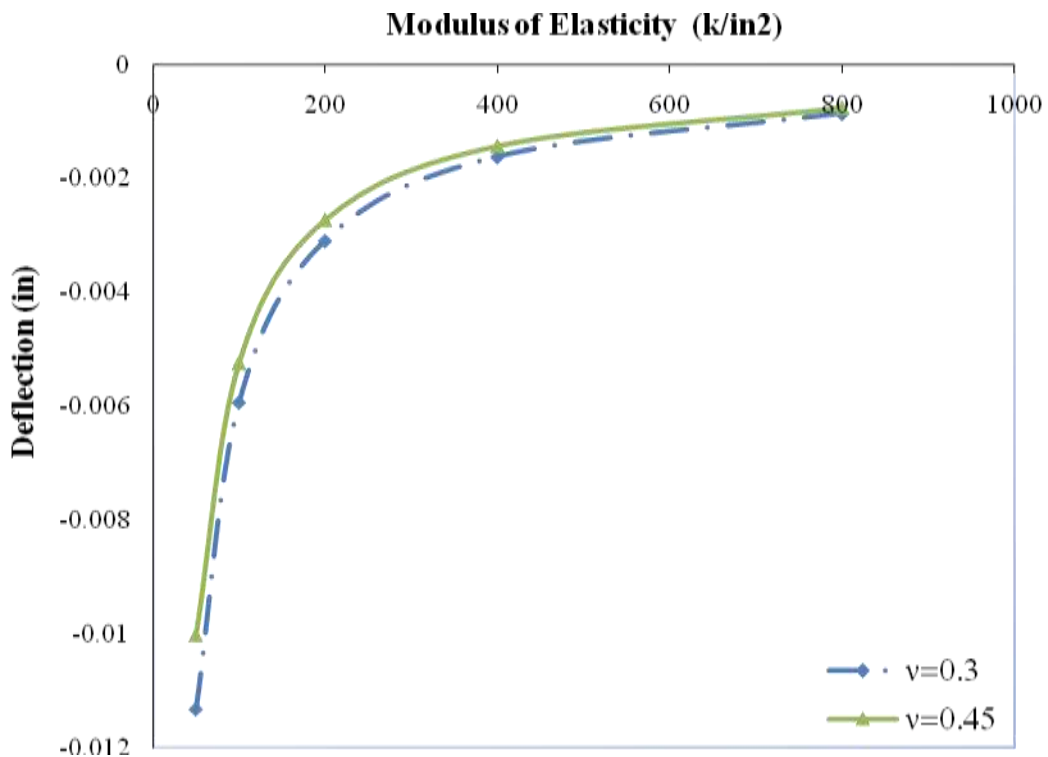


Figure 6.6 Deflection as a function of Solid Elastic parameters (E, ν)

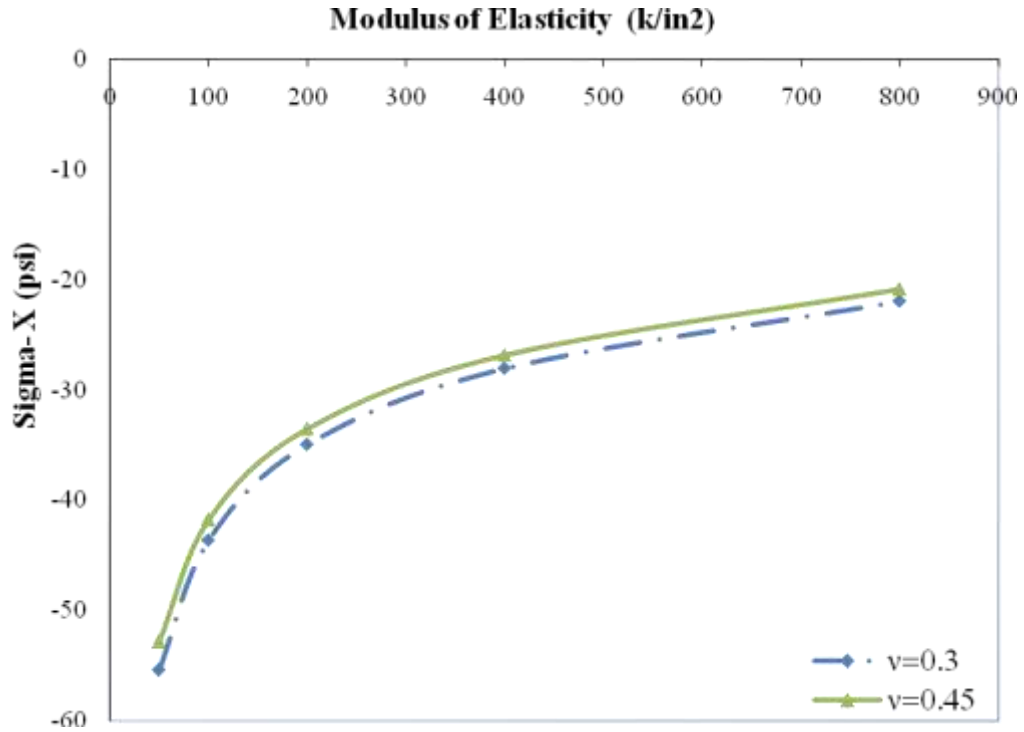


Figure 6.7 Longitudinal stress in the X direction as a function of Solid Elastic parameters (E, ν)

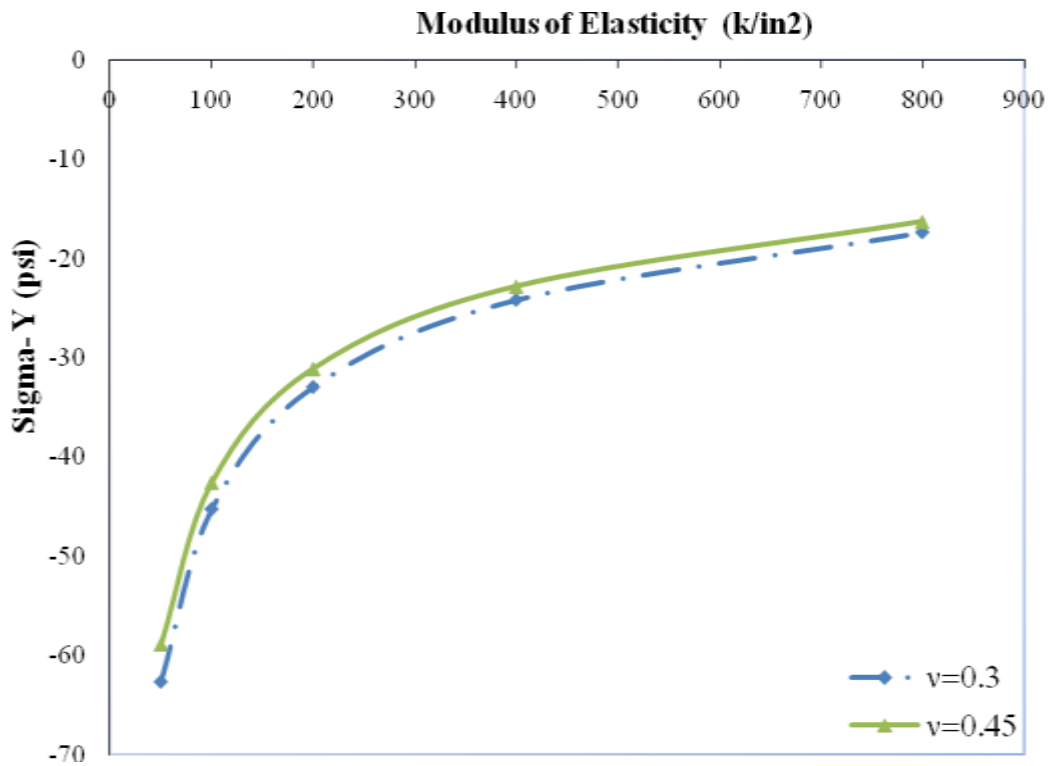


Figure 6.8 Longitudinal stress in the X direction as a function of Solid Elastic parameters (E, ν)

6.2 FOUNDATION MODEL

The objective of this study was to compare the general response of the baseline case described above under different foundation models (Winkler, Vlasov and Solid Elastic). Since it is not possible to find equivalent foundation parameters for the three models, this study will only serve the purpose of verifying that NYSlab captures the differences between them.

For this comparison study, the modulus of subgrade reaction of the Winkler foundation was set to 200 psi/in., the Vlasov model used the same modulus of subgrade reaction as the Winkler model with a shear modulus of 30 kip/in. Through trial and error, a Boussinesq foundation with a modulus of 20 ksi and a Poisson ratio of 0.3 agreed well with the stresses of the other foundation types.

The foundation is expanded beyond the edge of the slabs for the Vlasov and Solid Elastic foundations to capture the foundation deformation beyond the edge. This has a stiffening effect that reduces the deflection of the edge of the slabs. Figure 6.9 shows contours of the deformation of the top of the foundation for the Vlasov and Winkler foundations illustrating the existence of foundation beyond the edge of the slabs in NYSlab. This figure also shows the discontinuity of deflections on the Winkler foundation because of its assumed dense liquid behavior.

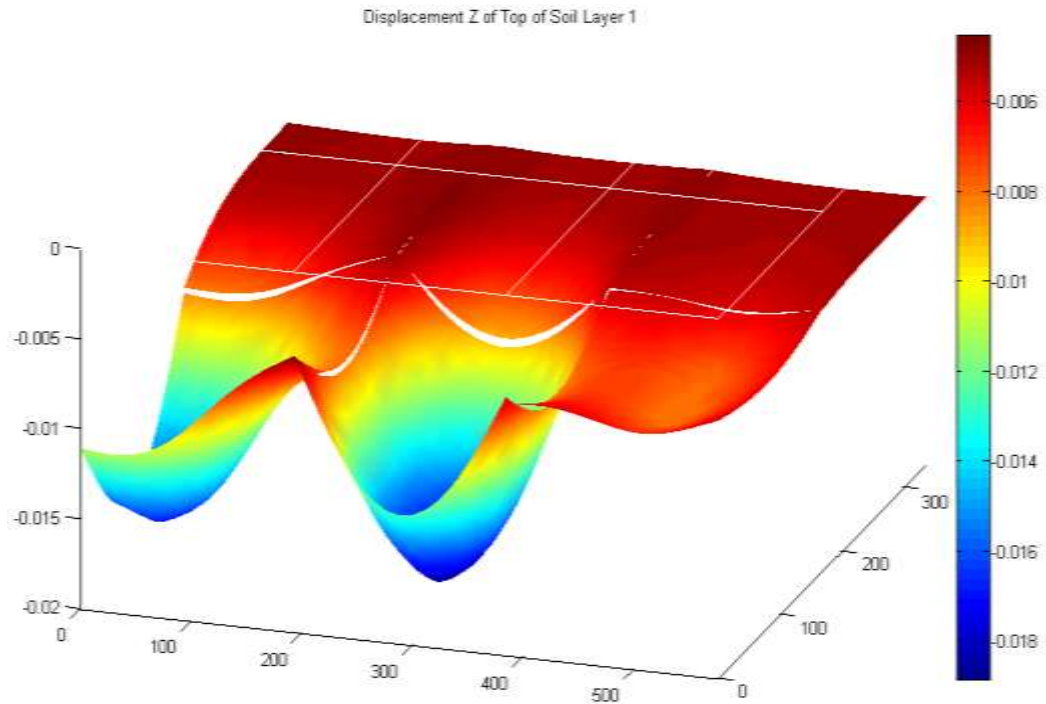
The behaviors of the slabs for the three foundation models studied for the effects of shear stiffness in the Vlasov model and the elastic parameters of the Solid Elastic foundation. The slab deflections for the three foundation models are shown in Figure 6.10. The effect of the extension of the foundation beyond the edge of the slab is quite apparent. The deflections with the Vlasov model at the edges are significantly lower than with the Winkler model. This difference cannot be attributed to the shear parameter but is the effect of the added foundation stiffness caused by the extension of the foundation. This foundation extension also has the effect of changing the curvature of deformation close to the edge of the slab. This translates into larger slab stresses for the Vlasov and Solid Elastic foundation when compared to the Winkler foundation as seen in Figure 6.11.

6.3 SLAB DIMENSIONS

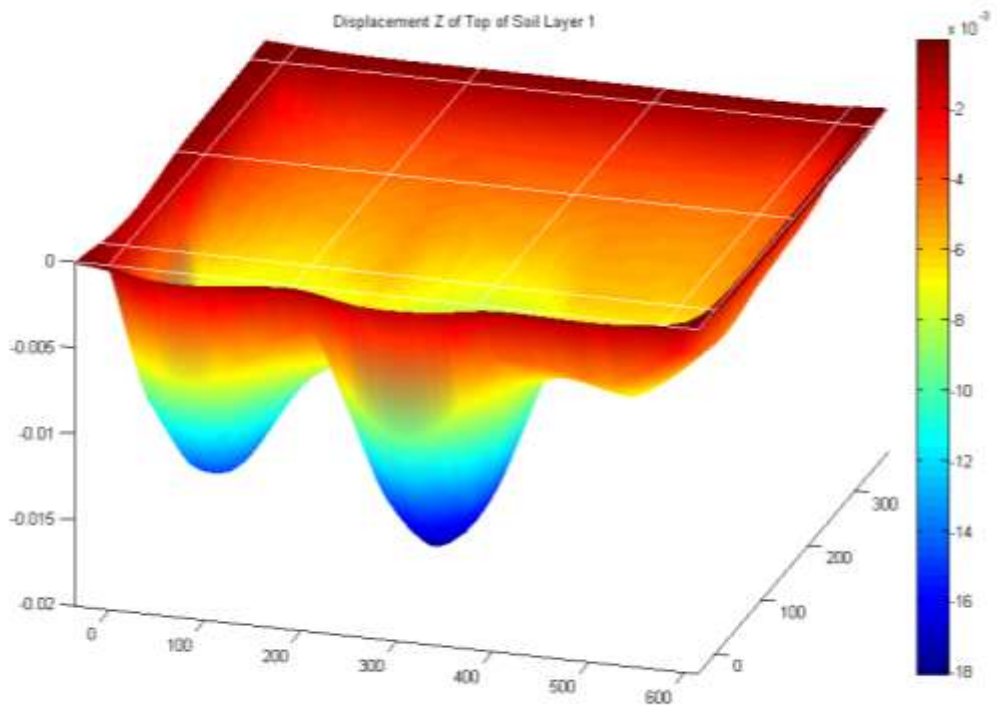
For this study, the length, width and thickness of slabs placed on two types of foundations (Winkler and Vlasov) were varied. The effects of these parameters on the responses of the slabs are discussed in the following section.

6.3.1 Slab Length and Width

To quantify the effects of the slab dimensions on deflections and stresses, the length of the slabs was varied from 12 ft to 20 ft. Three different widths of slabs (12 ft, 14 ft and 16 ft) were considered. The truck was placed in the middle of the first row of the slabs for all cases. In other words, the first triple-axle was placed in the middle of the second slab of the first row of slabs. Figures 6.12 and 6.13 show the results for absolute maximum deflections, and stresses in the X- and Y-directions.



(a) Winkler Foundation Deflection



(b) Vlasov Foundation Deflection

Figure 6.9 Effect of extending the foundation beyond the edge of the slab in the Vlasov model

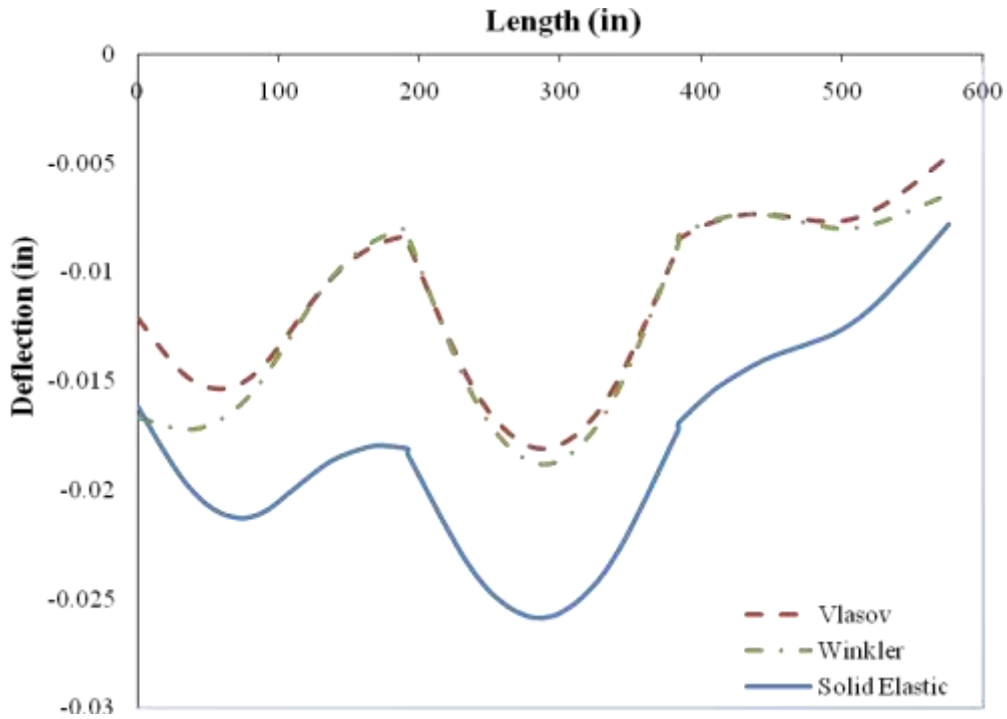


Figure 6.10 Comparison of deflections under the Winkler, Vlasov and Solid Elastic foundations

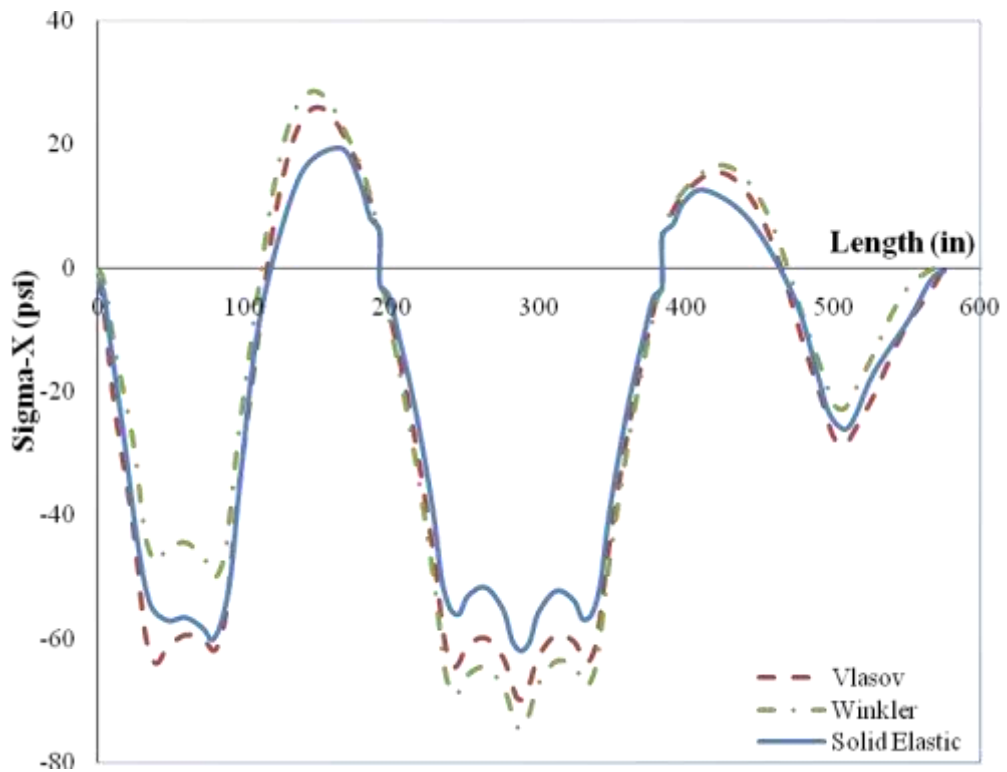
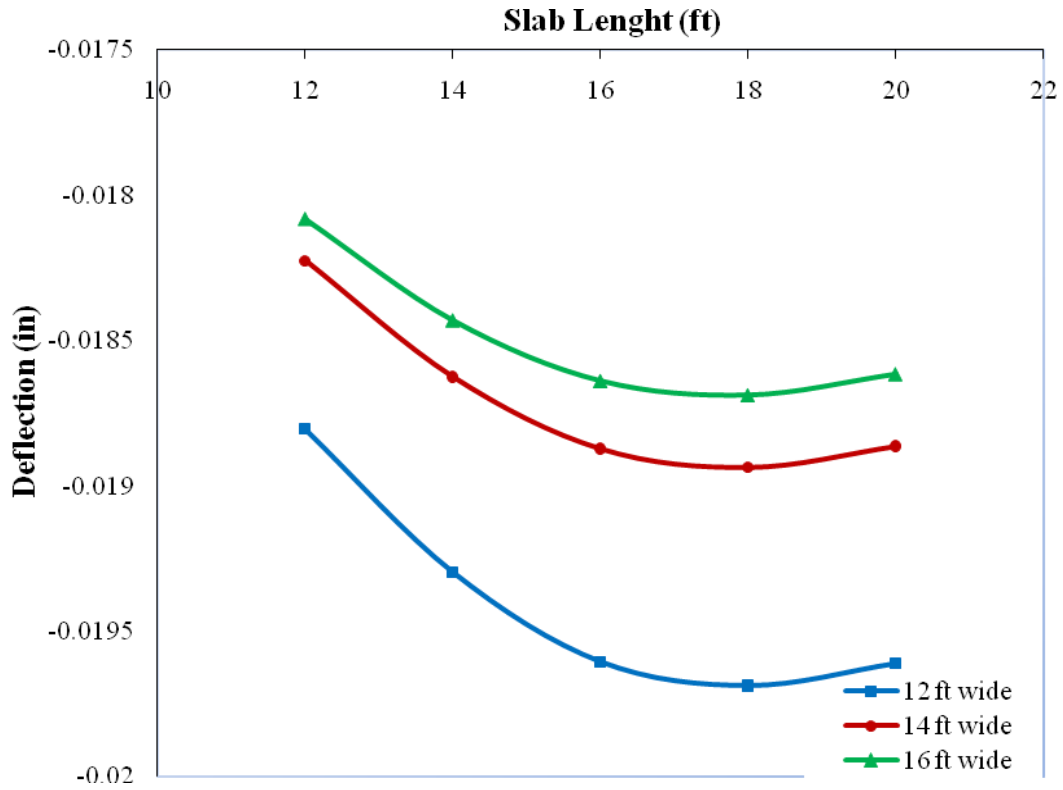
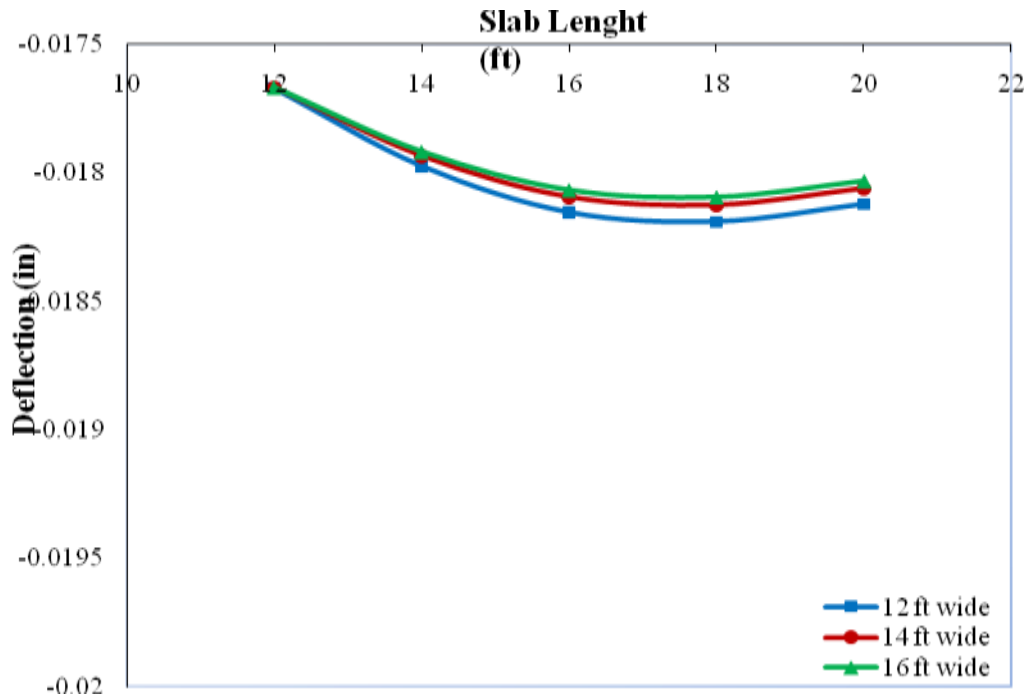


Figure 6.11 Comparison of bending stresses (in X direction) under the Winkler, Vlasov and Solid Elastic



(a) Winkler Foundation Deflection



(b) Vlasov Foundation Deflection

Figure 6.12 Deflection as a function of slab dimensions

As shown in Figure 6.12, increasing the length up to 18 ft resulted in increased maximum deflections. This could be due to the increased flexibility of the longer slabs. For slab lengths larger than 18 ft, the slab deflections begin to decrease, as the fact that the load is spread over a larger area begins to dominate. This behavior is seen for all slab widths and foundation types.

The shear modulus of 30 ksi in the Vlasov foundation not only reduced the deflections relative to Winkler foundation, but it also decreased the impact of the slab dimensions. By increasing the slab dimensions for slabs placed over the Vlasov foundation, the absolute maximum deflections changed only by 3%, while the change in deflection under the Winkler foundation was 9%.

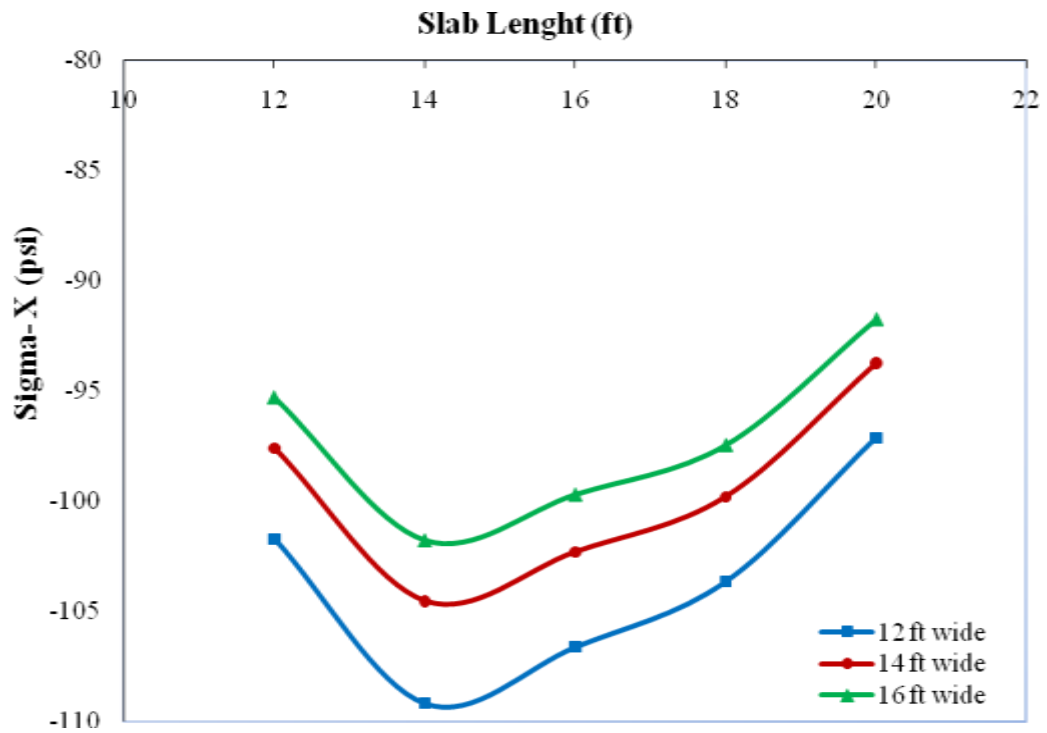
The longitudinal bending stresses show a similar behavior as seen in Figure 6.13. For short slabs with a length of 12 ft the stresses are small but as the length increases, the stresses increase up to a length of 14 ft. This increase in stresses is due to the increased moment-arm in the slightly longer slab. For lengths larger than 14 ft, the increased moment-arm has a smaller effect than the decreased contact stresses between the slab and foundation due to the larger contact area. This results in a reduction of stresses as the slab length increases beyond 14 ft. As expected, the stresses for the Vlasov foundation are less than those from the Winkler foundation due to the inclusion of shear stiffness in the Vlasov model.

6.3.2 Slab Thickness

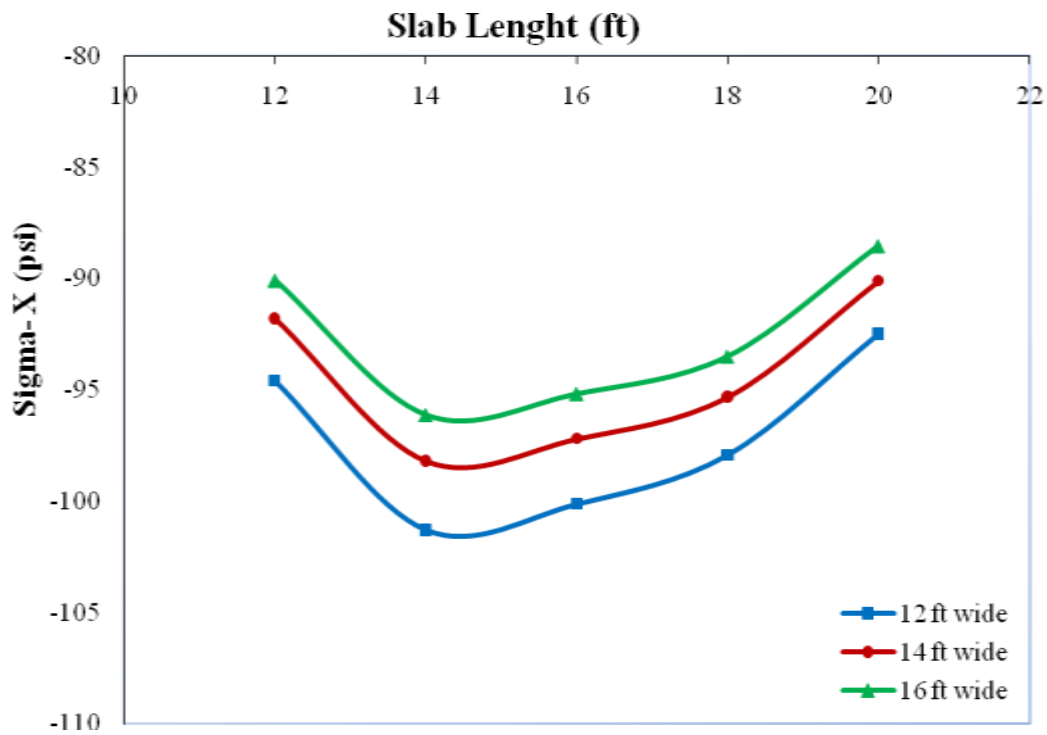
To study the effect of the thicknesses of the PCC layer on a Winkler foundation, the thickness was varied from 6 in. to 18 inches. As shown in Figure 6.14, the slab deflection decreased by increasing the thickness of the slab up to 18 in., because of the increase in the rigidity of the slab. For slabs thicker than 18 in., the weight of the slab becomes a dominant effect over the rigidity of the slab and the deflections begin to increase. Even though not shown here, for slabs thicker than 24 in., the maximum deflection occurred at the edge of the slab instead of the center of the slab. As expected and shown in Figure 6.15, the increase in the thickness of the slab resulted in a reduction in the stresses, especially for the stresses in the y direction.

6.3.3 Unbonded PCC Layers

As previously discussed, NYSlab is capable of analyzing a pavement with several layers of PCC and foundation. In this section the influence of considering an unbonded two-layer slab system on the performance of the pavement is evaluated. For this study, the total thickness of the two slabs was kept constant at 12 in. The thickness of the top PCC layer was varied from 2 in. to 10 in. The foundation was modeled as Winkler. The absolute maximum deflections and stresses of the top layer as a function of the thickness of the top PCC layer are shown in Figures 6.16 through 6.18. The results are normalized with respect to the corresponding values obtained from a 12-in. thick monotonic slab (ratio is of unbonded over monolithic slab performance variables). The deflection ratio reaches a maximum when both layers are 6 in thick. The plots for the longitudinal bending stresses also show the expected behavior. As the top layer increases in thickness, the stresses increase up to about 8 in after which the stresses begin to decrease. The stress ratio should be one when the top layer thickness is 12 in since the system becomes a one-layer pavement; the results do show this behavior. The behavior for the stress in the bottom layer shows the same expected trends.



(a) Winkler Foundation



(b) Vlasov Foundation

Figure 6.13 Longitudinal bending stress in the X direction as a function of slab dimensions

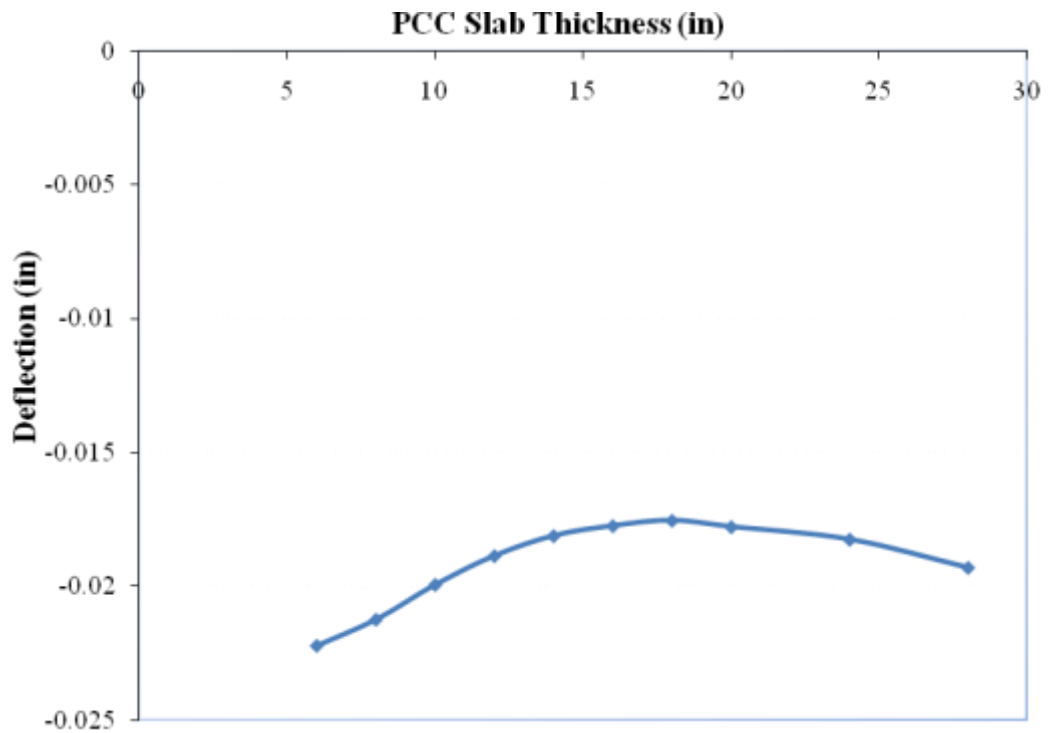


Figure 6.14 Deflection as a function of PCC layer thickness

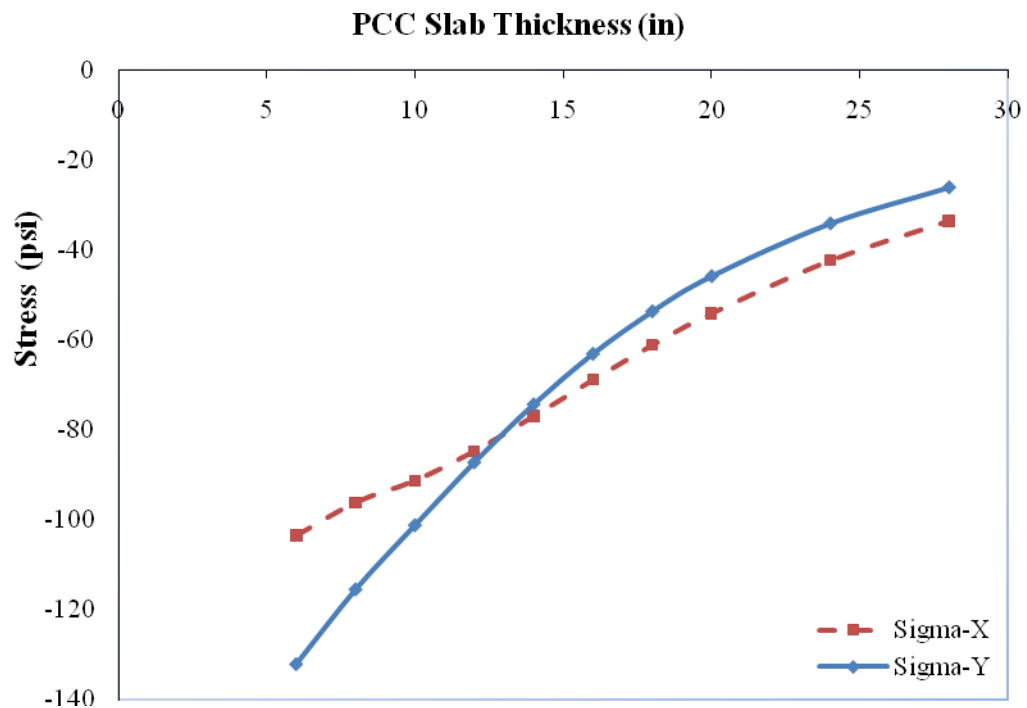


Figure 6.15 Longitudinal stresses as a function of of PCC layer thickness

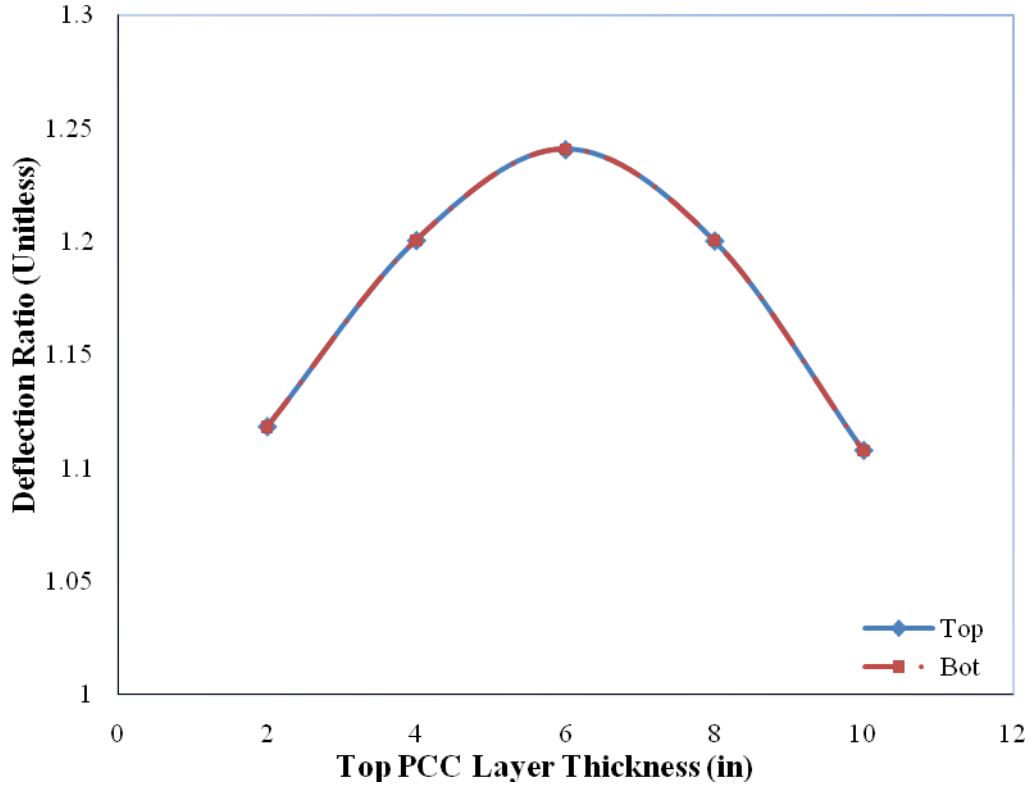


Figure 6.16 Deflection as a function of top PCC layer thickness

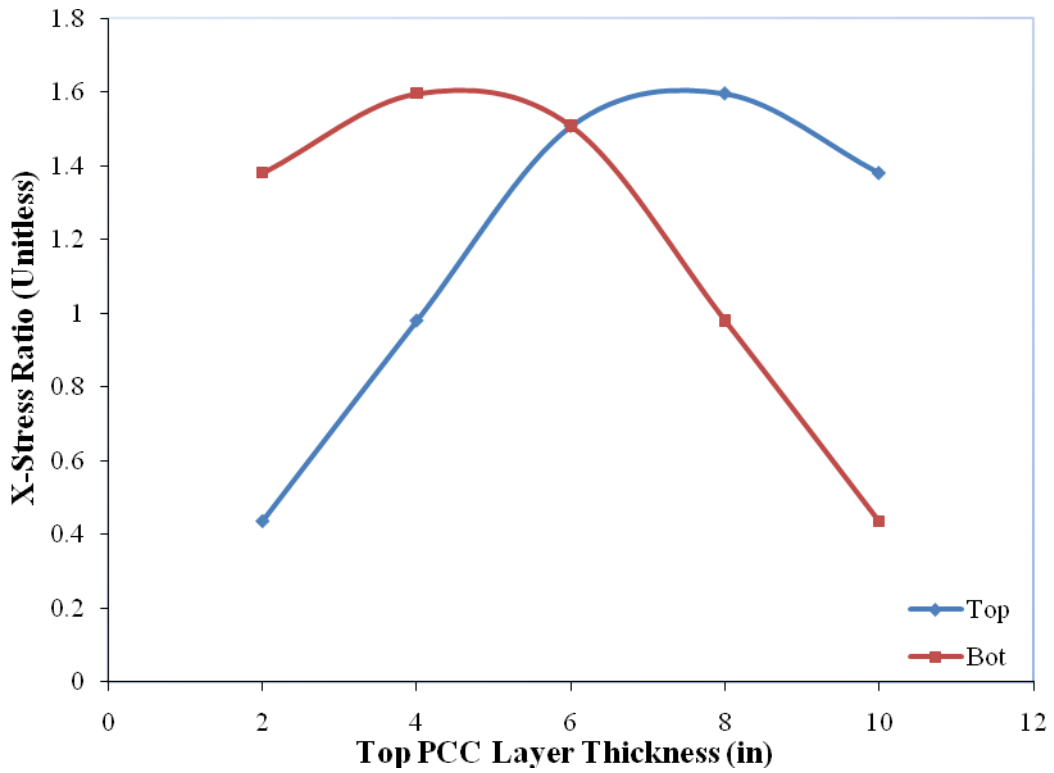


Figure 6.17 Longitudinal stress in the X direction as a function of top PCC layer thicknesses

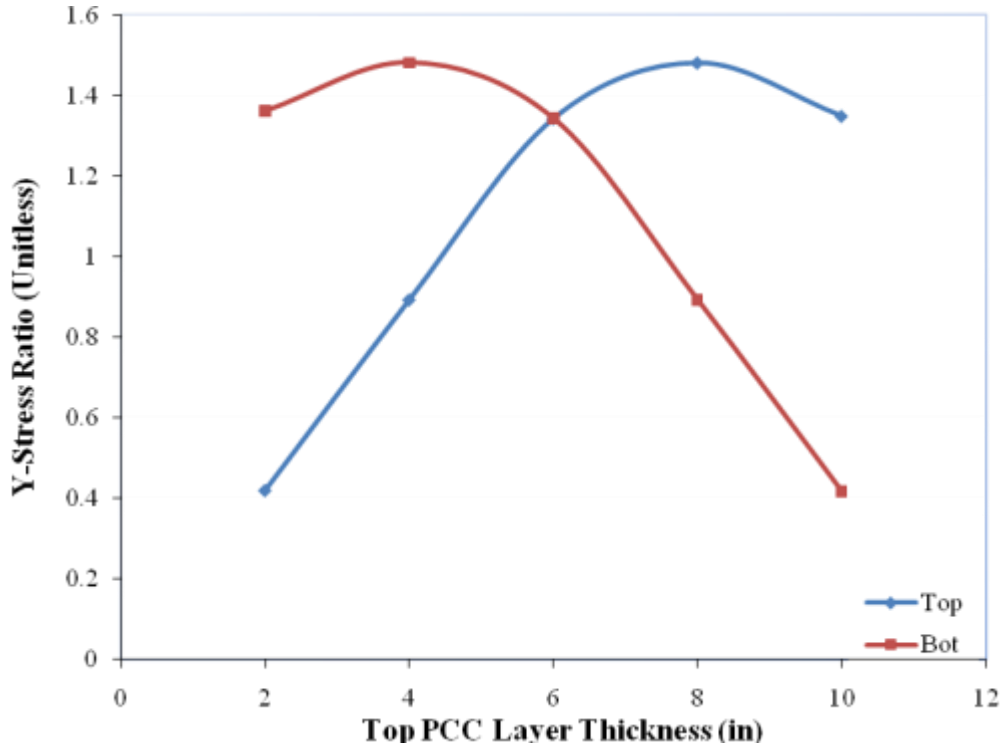


Figure 6.18 Longitudinal stress in the X direction as a function of top PCC layer thicknesses

6.4 THERMAL GRADIENT

To better predict pavement thermal loads, NYSlab is capable of modeling a non-linear thermal gradient across the thickness of the slabs. The gradient is modeled as:

$$\Delta t = a_0 + a_1 \times z + a_2 \times z^2 + a_3 \times z^3 \quad (6.1)$$

where, a_i can be fitted from field measurements at four points across the thickness of the slabs at specific pavement test sections. The origin of this equation is located at the “neutral plane”.

To verify the correct implementation of this model, a linear thermal gradient was first considered. Parameter a_1 was varied between $-1^\circ\text{F}/\text{in.}$ and $1^\circ\text{F}/\text{in.}$ while keeping all other coefficients equal to zero. A thermal expansion coefficient $\alpha=5\text{e-}6/^\circ\text{F}$ was assumed. As an example, an $a_1=1$ thermal gradient, represent a 12°F change through the thickness of the slab, in daytime, when the temperature on top of the pavement is higher than the bottom. Figure 6.19 shows the variation of maximum deflection as a function of the linear thermal gradient. When a_1 is positive, the pavement curls up (concave down) and produces a reduction in deflection. This figure demonstrates the expected linear relationship between thermal gradient and deflection [39]. Figure 6.20 shows the variation of the longitudinal bending stresses as a function of a_1 where an almost linear relationship is observed. As expected, the curling up of the pavement for positive a_1 produces an increase in stresses because of the reduction in the subgrade reaction (support) provided by the foundation. If there were no external and body forces, the stresses produced just by the thermal gradient would have been zero [39].

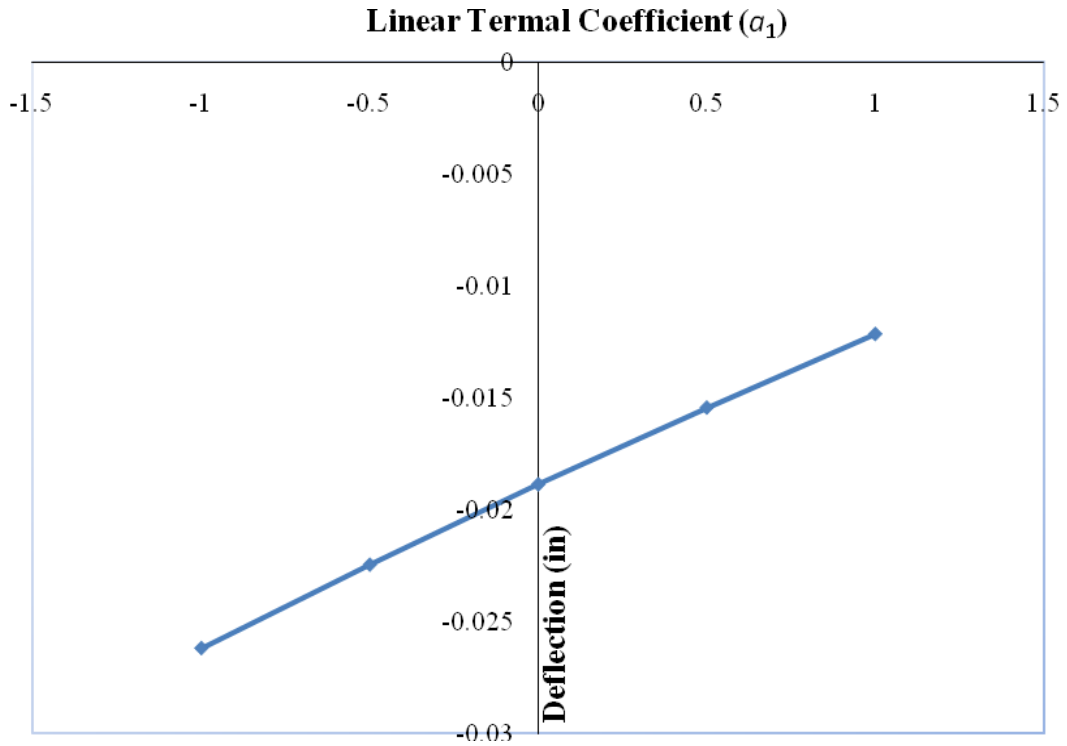


Figure 6.19 Maximum deflection as a function of Linear Thermal Coefficient (a_1)

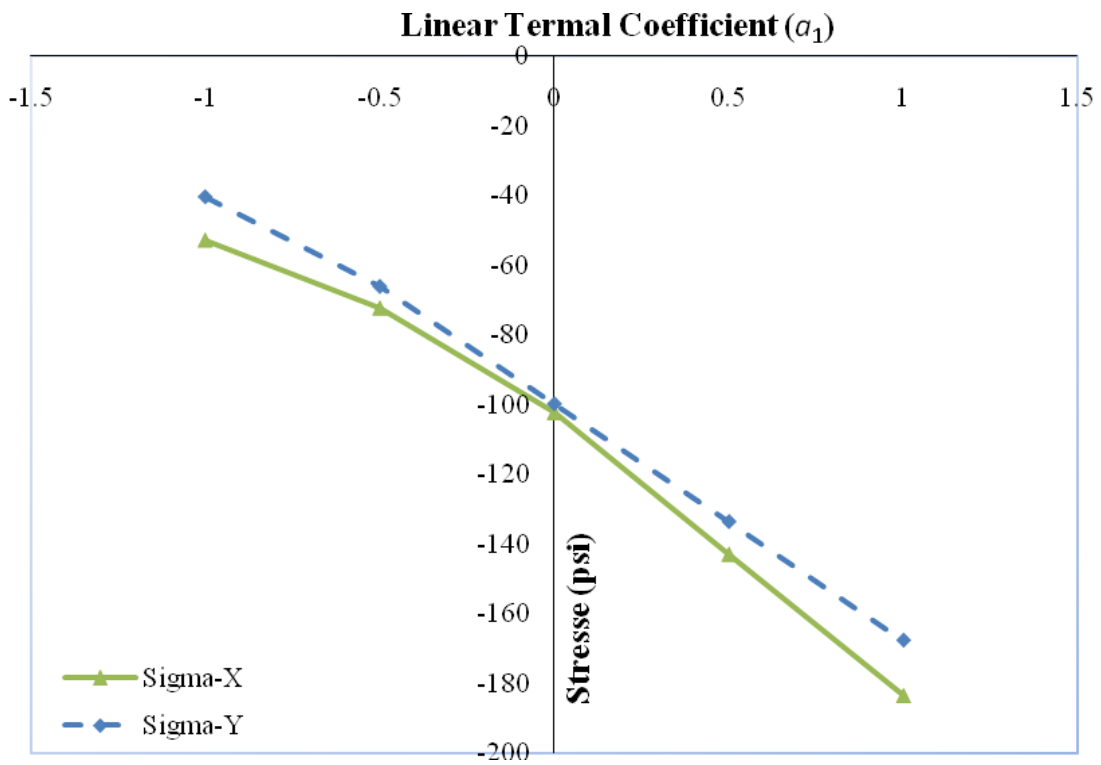


Figure 6.20 Maximum longitudinal stresses as a function of Linear Thermal Coefficient

To determine the effect of the quadratic coefficient in the thermal gradient equation, the parameter a_2 changed from -0.04 to $0.04^\circ\text{F}/\text{in.}^2$ while the linear parameter a_1 was set to $1^\circ\text{F}/\text{in.}$ and all other coefficients were fixed at zero. Figure 6.21 shows that the pavement deflection does not change when a_2 is varied. This is the expected behavior since the thermal moment produced

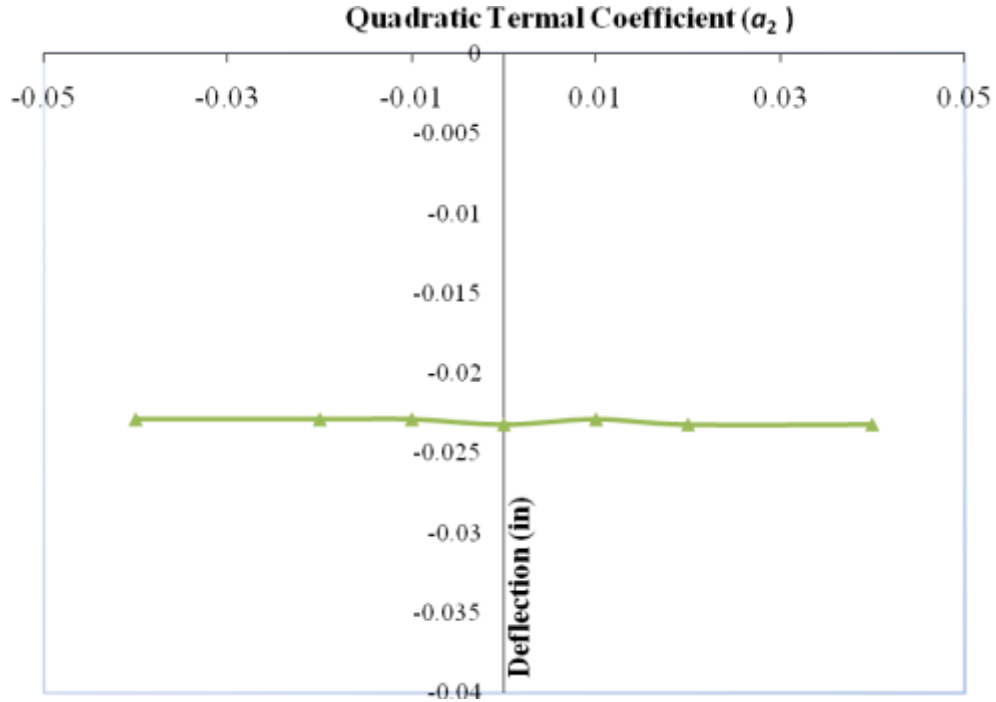


Figure 6.21 Maximum deflection as a function of Quadratic Thermal Coefficient (a_2)

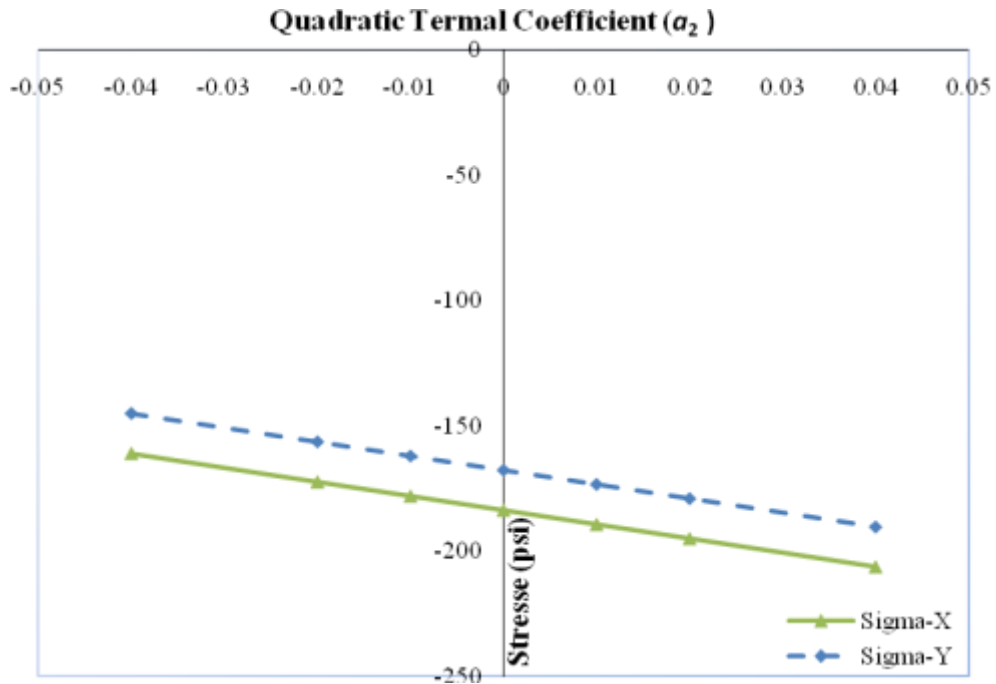


Figure 6.22 Maximum longitudinal stresses as a function of Quadratic Thermal Coefficient

by a quadratic thermal gradient profile is zero [39]. Figure 6.22 shows also the expected linear behavior for the variation of bending stresses [39]. The results of this section verify the correct numerical implementation of the non-linear thermal gradient in NYSlab. The implementation in NYSlab allows for a thermal gradient to exist in all PCC layers of the pavement, not only in the top one as in JSLAB2004.

CHAPTER 7: SUMMARY AND CONCLUSIONS

This report presents the development of NYSlab for the analysis of rigid pavements designed to improve the capabilities of JSLAB2004. The most significant improvements implemented in NYSlab over other software are: a) Finite Element model based on an isoparametric element that allows for the modeling of irregular geometries, b) no limitation in the number of PCC and foundation layers, c) more accurate modeling of the contact between unbonded PCC layers, PCC and foundation layers using Gap elements, d) foundation model extended beyond the edge of the slabs to more accurately model the edge deflections and stresses, and e) implementation of non-linear thermal gradient models applied to any number of PCC layers.

Uniform and non-uniform meshes were implemented and analyzed for convergence. The results showed that the deflection converges with less than 10 elements in each direction for both uniform and non-uniform meshes. A finer mesh of 16 elements in a non-uniform mesh and 30 elements for the uniform mesh are needed for convergence of stresses.

The effect of the element aspect ratio on convergence of the deflection and stresses was also studied. The aspect ratio of the elements did not seem to have a significant effect on the convergence of the deflection. On the other hand, increasing the aspect ratio of the elements changed the results for stresses only because at high aspect ratios, the number of elements in one direction dropped below the required for convergence.

The results produced by NYSlab were also compared with those of JSLAB2004 and ISLAB2000, using the same pavement and loading conditions. A good agreement in terms of deflections and stresses was observed between the three software packages. A small discrepancy was found in the deflection results of ISLAB2000 because it does not include the self-weight of the slab in the calculation.

To further verify the numerical implementation of the models, a parametric study was conducted. These parametric studies demonstrated that NYSlab accurately models the interplay between the pavement geometric characteristics, foundation parameters and the resulting deflections and stresses. Of significant importance was the improvement in the prediction of edge-of-slab deflections and stresses resulting from the extension of the foundation beyond the edge of the slabs included in NYSlab. Another major improvement in NYSlab was the implementation of a

model to predict the pavement response under a non-linear thermal gradient. The appropriate behavior of this model was also verified.

References

- [1] Buch, N., Gilland, D., Vongchusiri, K. and Van Dam, T. 2004, *A Preliminary Mechanistic Evaluation of PCC Cross-Sections Using Islab2000*, Final Research Report RC-1441, Michigan State University
- [2] Ceylan, H., Tutumluer, E. and Barenberg, E.J. 1999, *Artificial Neural Network Analysis of Concrete Airfield Pavements Serving The Boeing B-777 Aircraft*, 78th Annual Meeting of Transportation Research Board, Washington DC
- [3] Lukanen, E.O., 2005, *Load Testing of Instrumented Pavement Sections*, Final Technical Report, MN/RC-2005-47, University of Minnesota
- [4] Galaxy Scientific Corporation, 2004, *JSLAB (r2004) User Manual Upgrade Supplement*, Federal Highway Administration, Washington, DC
- [5] Huang, Y.H., 2004, *Pavement Analysis and Design*, Pearson Prentice Hall Inc.
- [6] Khazanovich, L., 2003, *Finite Element Analysis of Curling of Slabs on Pasternak Foundation*, 16th ASCE Engineering Mechanics Conference
- [7] Khazanovich, L., 1994, *Structural Analysis of Multi-Layered Concrete Pavement System*, PHD Thesis, University of Illinois at Urbana-Champaign
- [8] Khazanovich, L. and Gotlif, A., 2003, *Evaluation of Joint and Crack Load Transfer*, Federal Highway Administration FHWA-RD-02-088
- [9] Smith, K.D., Peshkin, D.G., Darter, M.I. and Mueller, A.L., 1990, *Performance of Jointed Concrete Pavements*, Volume III, Federal Highway Administration FHWA-RD-89-138
- [10] Ioannides, A.M., Thompson, M.R. and Barenberg, E.J., 1985, *Finite Element Analysis of Slabs-On-Grade Using a Variety of Support Models*. Proc., Third Int. Conference on Concrete Pavement Design and Rehabilitation, Purdue University, Apr., 309-324
- [11] Cheung, Y.K. and Zienkiewicz, O.C., 1965, *Plates and Tanks on Elastic Foundations: An Application of Finite Element Method*, Vol.1, pp.451-461

- [12] Huang, Y.H. and Wang, S.T., 1974, *Finite-Element Analysis of Rigid Pavements with Partial Subgrade Contact*, Transportation Research Record 485, pp.39-54, Transportation Research Board
- [13] *Structural Analysis Computer Programs for Rigid Multicomponent Pavement Structures with Discontinuities --WESLIQID and WESLAYER*. Report 3. Manual for the WESLAYER Finite element Program
- [14] Tabatabaie, A.M. and Barenberg, E.J., 1979, *Longitudinal Joint System in Slip Formed Rigid Pavements*, Vol.3; User's Manual, Report FAA-RD-79-4, III; U.S. Department of Transportation
- [15] Help Menu for ISLAB2000
- [16] *History of J-SLAB Development*, JSLAB2004 Software
- [17] Vlasov, V.Z. and Leontev, N.N., 1960, *Beams, Plates and Shells on Elastic Foundations*, NASA-NSF, NASA TT F-357, TT 65-50135, Israel Program for Scientific Translations (translation date: 1966)
- [18] Pronk, A.C., 1993, *The Pasternak foundation – An attractive alternative for the Winkler Foundation*, Proceedings of the 5th International Conference on Concrete Pavement Design and Rehabilitation, Vol. 1, Purdue University, West Lafayette, USA
- [19] Ioannides, A.M., and Korovesis. 1992, *Analysis and Design of Doweled Slab-on-Grade Pavement Systems*, Journal of Transportation Engineering, Vol. 118, No. 6, pp. 745–768
- [20] Jones, R. and Xenophontos, J., 1976, *On the Vlasov and Kerr Foundation Models*. Acta Mechanica 25 (1976), pp. 45–49
- [21] Khazanovich L.; Ioannides A.M., 1993, *Finite Element Analysis of Slabs-on-Grade Using Higher Order Subgrade Soil Models*, Airport Pavement Innovations Theory to Practice, American Society of Civil Engineers
- [22] NCHRP, 2003, *Structural Response Modeling of Rigid Pavements, (Appendix QQ- Guide for Mechanistic-Empirical Design Of New and Rehabilitated Pavement Structures)*, National Cooperative Highway Research Program, Transportation Research Board, National Research Council
- [23] Kerr, A.D., 1964, *Elastic & Viscoelastic Foundation Models*, Journal of Applied Mechanics.31, No. 3, 491-498
- [24] Pickett, G. and Ray, G.K., 1951, *Influence Charts for concrete Pavements*, Transactions, ASCE, Vol. 116
- [25] Tabatabaie, A.M. and Barenberg, E.J., 1980, *Structural Analysis of Concrete Pavement Systems*, ASCE, Transportation Engineering Journal. Vol. 106, No. 5, pp. 493-506
- [26] Hiller, J.E. and Buch, N., 2004, *Assessment of Retrofit Dowel Benefits in Cracked Portland Cement Concrete Pavements*, Journal of Performance of Constructed Facilities, ASCE, pp. 29-35

- [27] Cook R.D., Malkus D.S., Plesha M.E., Witt R.J., 2005, *Concepts and applications of FEA*, John Wiley and Sons, Inc., 4th Edition
- [28] Thompson, L.L. and Thangavelu, S.R., 2002, *A stabilized MITC Element for Accurate Wave Response in Reissner–Mindlin Plates*, *Comp. & Struct.*, 80(9-10):769-789
- [29] Ayvaz, Y. and Ozqan, K., 2002, *Application of Modified Vlasov Model To Free Vibration Analysis of Beams Resting on Elastic Foundations*, *Journal of Sound and Vibration*, Vol. 255, pp. 111–127
- [30] Shoukry, S.N. and William, G.W., 2001, *Identification of Critical Stress Concentration around Dowel Bars*, Report No. MUTC # 7, West Virginia University
- [31] Ioannides, A.M., 2006, *Concrete Pavement Analysis: The First Eighty Years*, *International Journal of Pavement Engineering*, Vol. 7, No. 4
- [32] Bhatti, M. A., 2006, *Advanced Topics in Finite Element Analysis of Structures with Mathematica and MATLAB Computations*, Wiley
- [33] Bathe, K.J. and Dvorkin, E.N., 1985, *A 4-Node Plate Bending Element Based on Mindlin/Reissner Plate Theory and A Mixed Interpolation*. *Int. J. Numer. Meth. Eng.* **21** 2, pp. 367–383
- [34] Bathe, K. J., 1982, *Finite Element Procedures in Engineering Analysis*, Prentice-Hall, Englewood Cliffs, NJ
- [35] Thompson, L.L., 2003, *On Optimal Stabilized MITC4 Plate Bending Elements for Accurate Frequency Response Analysis*, *Computers & Structures*, 81:995-1008
- [36] Scott, F. S., 1981, *Foundation Analysis*, Prentice-Hall, Englewood Cliffs, NJ
- [37] Stet, M., Cauwelaert, F.V., Beuving E., 1998, *Evaluation Method for Jointed Concrete Airfield Pavements*, Fourth International Workshop on Design Theories and Verification of Concrete Slabs for Pavements and Railroads
- [38] Deaton J.B., 2005, *A Finite Element Approach to Reinforced Concrete Slab Design*, Georgia Institute of Technology
- [39] Vinson J.R., 1999, *The Behavior of Sandwich Structures of Isotropic and Composite Materials*, Technomic
- [40] Ruiz J.M., Rasmussen R.O., Chang G.K., Dick J.C., Nelson P.K., 2005, *Computer-Based Guidelines for Concrete Pavements*, Volume II—Design and Construction Guidelines and HIPERPAV II User's Manual, Federal Highway Administration Report FHWA–HRT–04–122

[41] http://pavementinteractive.org/index.php?title=Aggregate_Interlock

[42] <http://www.angelfire.com/oh4/psychfea/gap2.html>